JOURNAL OF GEOPHYSICAL RESEARCH, VOL. 106, NO. D19, PAGES 23,073–23,095, OCTOBER 16, 2001

Global modeling of tropospheric chemistry with assimilated meteorology: Model description and evaluation

Isabelle Bey,[1] Daniel J. Jacob, Robert M. Yantosca, Jennifer A. Logan, Brendan D. Field, Arlene M. Fiore, Qinbin Li, Honguy Y. Liu, Loretta J. Mickley, and Martin G. Schultz[2]

Division of Engineering and Applied Sciences, and Department of Earth and Planetary Sciences, Harvard University, Massachusetts

Abstract. We present a first description and evaluation of GEOS-CHEM, a global three-dimensional (3-D) model of tropospheric chemistry driven by assimilated meteorological observations from the Goddard Earth Observing System (GEOS) of the NASA Data Assimilation Office (DAO). The model is applied to a 1-year simulation of tropospheric ozone-NO_x-hydrocarbon chemistry for 1994, and is evaluated with observations both for 1994 and for other years. It reproduces usually to within 10 ppb the concentrations of ozone observed from the worldwide ozonesonde data network. It simulates correctly the seasonal phases and amplitudes of ozone concentrations for different regions and altitudes, but tends to underestimate the seasonal amplitude at northern midlatitudes. Observed concentrations of NO and peroxyacetylnitrate (PAN) observed in aircraft campaigns are generally reproduced to within a factor of 2 and often much better. Concentrations of HNO_3 in the remote troposphere are overestimated typically by a factor of 2-3, a common problem in global models that may reflect a combination of insufficient precipitation scavenging and gas-aerosol partitioning not resolved by the model. The model yields an atmospheric lifetime of methylchloroform (proxy for global OH) of 5.1 years, as compared to a best estimate from observations of 5.5 +/– 0.8 years, and simulates H_2O_2 concentrations observed from aircraft with significant regional disagreements but no global bias. The OH concentrations are ~20% higher than in our previous global 3-D model which included an UV-absorbing aerosol. Concentrations of CO tend to be underestimated by the model, often by 10-30 ppb, which could reflect a combination of excessive OH (a 20% decrease in model OH could be accommodated by the methylchloroform constraint) and an underestimate of CO sources (particularly biogenic). The model underestimates observed acetone concentrations over the South Pacific in fall by a factor of 3; a missing source from the ocean may be implicated.

1. Introduction

Global three-dimensional (3-D) models of tropospheric chemistry are fast becoming standard tools for improving our knowledge of chemical budgets and processes in the troposphere. They are also beginning to be used in an exploratory way to provide chemical forecasts for experimental field programs [*Flatoy et al.*, 2000], to provide a prioris for satellite retrievals [*Palmer et al.*, 2001], to examine aerosol-chemistry-climate interactions [*Roelofs et al.*, 1997; *Mickley et al.*, 1999; *Adams et al.*, 2001], and to guide international environmental policy assessments [*Intergovernmental Panel on Climate Change (IPCC)*, 1995, 2001]. Several community intercomparisons of global tropospheric chemistry models have been conducted recently, demonstrating the rapid growth of the field [*Jacob et al.*, 1997; *Kanakidou et al.*, 1999; *Rasch et al.*, 2000; *IPCC*, 2001].

A central theme in the development of global tropospheric chemistry models is the simulation of ozone-NO_x-hydrocarbon chemistry. Better understanding of the factors controlling tropospheric ozone is a major research priority [*World Meteorological Organization (WMO)*, 1998]. More generally, ozone-NO_x-hydrocarbon chemistry determines radical and oxidant processes in the troposphere and lies therefore at the heart of most problems affecting tropospheric composition. Simulation of ozone-NO_x-

[1]Now at Swiss Federal Institute of Technology, Lausanne, Switzerland.

[2]Now at Max-Planck-Institut für Meteorologie Hamburg, Germany.

Paper number 2001JD000807.
0148-0227/01/2001JD000807$09.00

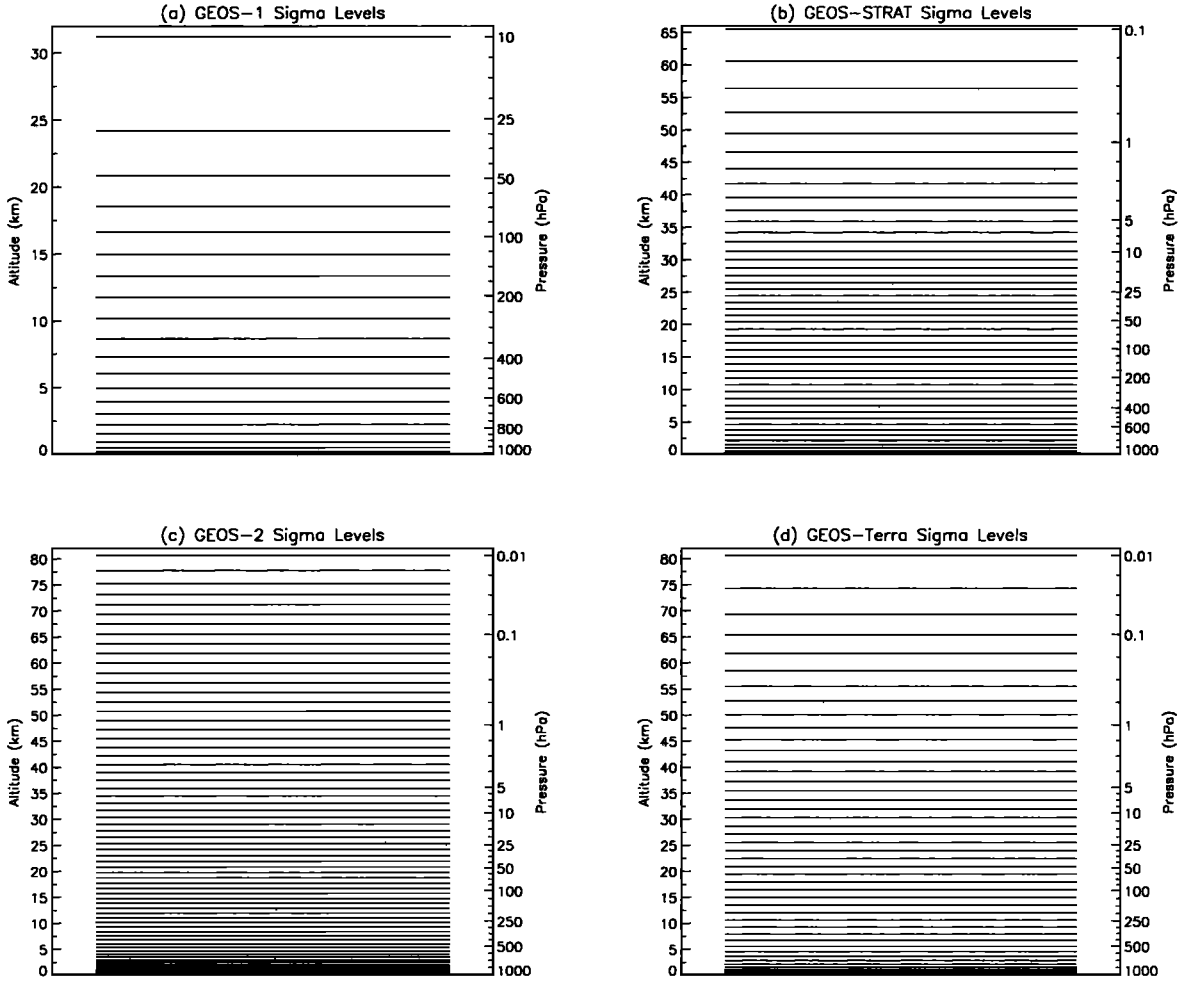

Figure 1. Sigma vertical levels in successive generations of the GEOS assimilated meteorological data. The GEOS-1 data (1985-1995) have 20 levels from the surface to 10 hPa; the GEOS-STRAT data (1996-1997) have 46 levels from the surface to 0.1 hPa; the GEOS-2 data (1998-1999) have 70 levels from the surface to 0.01 hPa; the GEOS-Terra data (2000-) have 48 levels from the surface to 0.01 hPa.

hydrocarbon chemistry is difficult in a global model because of the large number of species involved (~100), the nonlinearity of the chemistry, the numerical stiffness of the system, and the coupling of chemistry to transport over a wide range of scales. A number of independently developed models have been reported in the literature over the past few years [e.g., *Collins et al.*, 1997; *Brasseur et al.*, 1998; *Wang et al.*, 1998a; *Lawrence et al.*, 1999; *Levy et al.*, 1999; *Lelieveld and Dentener*, 2000]. They share similar theoretical foundations but differ in many ways including resolution, the driving meteorological fields, and the approaches and detail for simulating emissions, chemical processes, and deposition.

Our first-generation global model of tropospheric ozone-NO_x-hydrocarbon chemistry was described and evaluated by *Wang et al.* [1998a,1998b] and subsequently refined by *Horowitz and Jacob* [1999] and *Mickley et al.* [1999]. It uses meteorological fields from a general circulation model (GCM) developed at the Goddard Institute of Science Studies (GISS) [*Hansen et al.*, 1983; *Rind and Lerner*, 1996]. We have since developed the need for a model driven by assimilated meteorological observations in order to provide better constraints on the simulation of specific years, to allow investigations of interannual variability, and to set in place a machinery to conduct chemical forecasts in support of aircraft missions.

We present here our second-generation global model using assimilated meteorological data from the Goddard Earth Observing System (GEOS) of the NASA Data Assimilation Office (DAO) [*Schubert et al.*, 1993]. Development of this second-generation model involved the grafting of the *Wang et al.* [1998a] modules of photochemistry, emissions and deposition onto the original GEOS chemical transport model developed by *Allen et al.* [1996a,1996b] and *Lin and Rood* [1996]. We give in the present paper a general description and evaluation of the resulting model, which we call GEOS-CHEM, focusing on tropospheric ozone-NO_x-hydrocarbon chemistry. This paper is intended to provide background for

several recent and ongoing studies using the GEOS-CHEM model [*Singh et al.*, 2000a; *Li et al.*, 2000; *Palmer et al.*, 2001; *Liu et al.*, 2001; *Bey et al.*, this issue].

2. Model Description

2.1. Model Framework

The GEOS assimilated meteorological observations used to drive the GEOS-CHEM model are available as a continuous archive from 1985 to present, with 3- or 6- hour temporal resolution depending on the variable. The GEOS assimilation system has gone through successive generations: GEOS-1 (1985-1995), GEOS-STRAT (1996-1997), GEOS-2 (1998-1999), and GEOS-Terra (2000-). The horizontal resolution is 1° latitude by 1° longitude in GEOS-Terra and 2° latitude by 2.5° longitude in earlier versions. Meteorological fields are provided on a sigma coordinate with 20 vertical levels in GEOS-1, 26 in GEOS-STRAT, 70 in GEOS-2, and 48 in GEOS-Terra (Figure 1). The GEOS-CHEM model is presently used at Harvard with either GEOS-1, GEOS-STRAT, or GEOS-Terra products. Table 1 lists the GEOS variables used as input to the model. For computational expediency we frequently merge levels in the stratosphere and average the data horizontally over a 4°×5° grid. The model transports 24 chemical tracers to describe tropospheric O_3-NO_x-hydrocarbon chemistry (Table 2). Advection is computed every 15 min (2°×2.5° horizontal resolution) or 30 min (4°×5° horizontal resolution) with a flux-form semi-Lagrangian method described by *Lin and Rood* [1996]. Moist convection is computed using the GEOS convective, entrainment, and detrainment mass fluxes as described by *Allen et al.* [1996a,1996b]. We assume full mixing within the GEOS-diagnosed atmospheric mixed layer generated by surface instability.

2.2. Emissions

We present in this paper a simulation for 1994, and emissions for that year are given in Table 3. Simulations for other years use adjusted anthropogenic emissions, as described below.

2.2.1. Anthropogenic emissions Simulation of specific years with a global tropospheric chemistry model must take into account the year-to-year variability of anthropogenic emissions. We use a base emission inventory for 1985 described by *Wang et al.* [1998a] that includes NO_x emissions from the Global Emission Inventory Activity (GEIA) [*Benkovitz et al.*, 1996], nonmethane hydrocarbon (NMHC) emissions from *Piccot et al.* [1992], and CO emissions developed at Harvard. We scale these emissions for specific years as follows. For unregulated countries (where no regulations have been imposed to limit emissions), NO_x emissions are scaled using trends in CO_2 emissions from

Table 1. GEOS Fields Used as Input to the GEOS-CHEM Model

Variable	Resolution [a]	Application
Wind vector	Inst 6 h	advection
Surface pressure	Inst 6 h	advection
Wet convective mass flux, detrainment[b]	Avg 6 h	convection
Mixed layer depth	Avg 3 h	boundary layer mixing
Temperature	Inst 6 h	chemistry
Specific humidity	Inst 6 h	chemistry
Cloud optical depth[b]	Avg 6 h	photolysis
Surface albedo	Inst 6 h	photolysis, dry deposition (snow cover)
Land-Water indices	Inst 6 h	dry deposition, lightning
Sensible heat flux	Avg 3 h	dry deposition
Solar radiation flux at surface	Avg 3 h	dry deposition
Surface air temperature	Avg 3 h	dry deposition, biogenic emissions
Surface wind (10 m altitude)	Avg 3 h	dry deposition, NO_x soil emissions
Friction velocity	Avg 3 h	dry deposition
Roughness height	Avg 3 h	dry deposition
Water condensation rate[c]	Avg 6 h	wet deposition
Total precipitation at the ground	Avg 3 h	wet deposition
Convective precipitation at the ground	Avg 3 h	wet deposition
Column cloud fraction[d]	Avg 3 h	biogenic emissions

[a]The fields are given with three different temporal resolutions. "Inst 6 h" indicates that the quantity is an instantaneous value given every 6 hours. "Avg 6 h" and "Avg 3 h" indicate that the quantity is averaged over 6 and 3 hours, respectively.

[b]Vertically resolved.

[c]Actually provided as the change in specific humidity due to moist processes. Interpretation as a water condensation rate is approximate [*Liu et al.*, 2001].

[d]Used to separate the direct and diffuse photosynthetically active radiation (PAR) in the calculation of isoprene emissions.

Table 2. Tracers for GEOS-CHEM Model Simulation of Tropospheric Ozone-NO_x-Hydrocarbon Chemistry

Tracer	Composition
O_x	$O_3 + O + NO_2 + 2\times NO_3$
NO_x	$NO + NO_2 + NO_3 + HNO_2$
HNO_3	
HNO_4	
N_2O_5	
PAN	peroxyacetyl nitrate
H_2O_2	
CO	
C_2H_6	
C_3H_8	
ALK4	lumped $\geq C_4$ alkanes
PRPE	lumped $\geq C_3$ alkenes
Isoprene	
Acetone	
CH_3OOH	
CH_2O	
CH_3CHO	
RCHO	lumped $\geq C_3$ aldehydes
MEK	lumped $\geq C_4$ ketones
Methyl vinyl ketone	
Methacrolein	
MPAN	peroxymethacryloyl nitrate
PPN	lumped peroxyacyl nitrates[a]
R4N2	lumped alkyl nitrates

[a] Other than peroxyacetyl nitrate (PAN) and peroxymethacryloyl nitrate (MPAN).

fossil fuel combustion, and CO and NMHC emissions are scaled using trends in CO_2 emissions from liquid fuels. Yearly CO_2 emissions for individual countries are provided by *Marland et al.* [1999], who primarily used energy statistics published by the United Nations [1998]. For regulated countries we use other emission inventories such as those provided by the Environmental Protection Agency (EPA) for the United States [*EPA*, 1997] and the European Monitoring and Evaluation Program (EMEP) for European countries [*EMEP*, 1997]. Table 4 shows the evolution of CO and NO_x emissions between 1985 and 1994 for different geopolitical regions. Global CO and NO_x emissions show little change over the years, but European emissions decrease while emissions in Asia, Africa, and Oceania increase. The large decrease of emissions in Europe after 1991 is due to regulatory control but also to the collapse of the former USSR. The largest increase of emissions occurs in Asia.

2.2.2. Biomass burning emissions Biomass burning and wood fuel emissions are from a climatological inventory previously described by *Wang et al.* [1998a]. This inventory includes different categories of burning (forest wildfires, tropical deforestation, slash-and-burn agriculture, savanna burning, and burning of agriculture waste), and yields a global CO emission of 520 Tg CO yr^{-1}. Emissions of NO_x and hydrocarbons are derived from the CO inventory using emission ratios as described by *Wang et al.* [1998a]. Wood fuel emissions of CO account for an additional total of 133 Tg CO yr^{-1}.

2.2.3. Biogenic emissions Isoprene emission rates from vegetation in the *Wang et al.* [1998a] model were computed with a modified version of the GEIA inventory [*Guenther et al.*, 1995], the principal modifications being a decrease in the leaf area index (LAI) from tropical forests and an improved representation of light attenuation within the forest canopy. We have made here some additional modifications. On the basis of recent estimates of isoprene fluxes for tropical vegetation [*Klinger et al.*, 1998; *Helmig et al.*, 1998], and also to improve agreement between simulated and observed isoprene concentrations, we have reduced emission rates for several ecosystems (tropical rain forest, tropical montane, tropical seasonal forest, dry taiga) by a factor of 3. This leads to a global emission rate for isoprene of 397 Tg C yr^{-1}. A biogenic source of acetone scaled to isoprene emissions was previously included by *Wang et al.* [1998a]. Because monoterpene oxidation has since been recognized to represent a major source of acetone [*Reissel et al.*, 1999], we now distribute biogenic emissions of acetone (15 Tg C yr^{-1}) following the pattern of monoterpene emissions [*Guenther et al.*, 1995] rather than isoprene emissions. Monoterpene emissions are not directly included in the model because their effect on global ozone chemistry is minimal.

2.3. Chemistry

The chemical mechanism for the troposphere includes 80 species and over 300 reactions with detailed pho-

Table 3. Global Emissions for 1994 in the GEOS-CHEM Model

Species	Emission Rate
NO_x, Tg N yr^{-1}	
Fossil fuel combustion	22.8
Biomass burning	12
Soil	6.7
Lightning	3.4
Aircraft	0.5
Stratosphere	0.2
Total	45.6
CO, Tg CO yr^{-1}	
Fossil fuel combustion and industry	388
Wood fuel combustion	133
Biomass burning	522
Total	1043
Isoprene, Tg C yr^{-1}	
Vegetation	397
Ethane, Tg C yr^{-1}	
Industrial	6.6
Biomass burning	3.0
Total	9.6
Propane, Tg C yr^{-1}	
Industrial	7.0
Biomass burning	0.9
Total	7.9
$\geq C_4$ alkanes, Tg C yr^{-1}	
Industrial	31.2
$\geq C_3$ alkenes, Tg C yr^{-1}	
Industrial	11.8
Biogenic sources	11.3
Biomass burning	6.0
Total	29.1
Acetone, Tg C yr^{-1}	
Industrial	1.1
Biomass burning	8.7
Biogenic sources	15
Total	24.8

Table 4. Evolution of Anthropogenic Emission Rates Between 1985 and 1994

Species	1985	1991	1994
NO_x, Tg N yr^{-1}			
North America	6.2	6.4	6.5
South America	1.3	1.4	1.5
Europe	7.6	7.5	7.0
Africa	1.3	1.5	1.6
Asia	4.1	5.1	5.5
Oceania	0.5	0.6	0.7
Total	21	22.5	22.8
CO, Tg CO yr^{-1}			
North America	109.5	96.5	94.0
South America	21.0	23.0	24.5
Europe	153.0	145.5	123.0
Africa	18.0	19.5	22.0
Asia	82.0	103.5	113.5
Oceania	9.0	10.0	11.0
Total	392.5	398.0	388.0

Anthropogenic emissions include fossil fuel combustion and industrial sources. North America includes the United States and Canada. South America includes also Central America. Europe includes the former USSR. Africa includes the Middle East. Oceania includes Australia, Indonesia and New Zealand.

tooxidation schemes for major anthropogenic hydrocarbons and isoprene, as described by *Horowitz et al.* [1998]. It has been updated with recent experimental data from *DeMore et al.* [1997], *Atkinson* [1997] and *Brown et al.* [1999a,1999b]. We have also changed the fate of the hydroxy organic nitrates produced by isoprene oxidation. Because these compounds are now believed to decompose quickly to HNO_3 on surfaces [*Chen et al.*, 1998], we assume direct formation of HNO_3 instead of the organic nitrates. The effect of heterogeneous chemistry on tropospheric ozone has been reviewed by *Jacob* [2000]. Following his recommendations, we include four reactions: $NO_2 \rightarrow 0.5\ HNO_3 + 0.5\ HNO_2$, $NO_3 \rightarrow HNO_3$, $N_2O_5 \rightarrow 2\ HNO_3$, and $HO_2 \rightarrow 0.5\ H_2O_2 + 0.5\ O_2$, using reaction probabilities of 10^{-4} for NO_2, 10^{-3} for NO_3, 0.1 for N_2O_5, and 0.2 for HO_2. Aerosol surface areas are estimated on the basis of global 3-D sulfate concentration fields with monthly resolution from *Chin et al.* [1996], as described by *Wang et al.* [1998a].

Photolysis frequencies in the troposphere are calculated with the Fast-J algorithm of *Wild et al.* [2000], which uses a seven-wavelength quadrature scheme and accounts accurately for Mie scattering by clouds. Surface albedo and vertically resolved cloud optical depths are taken from the GEOS meteorological archive with 6-hour resolution. The model as described here uses climatological ozone concentrations as a function of latitude, altitude, and month to calculate the absorption of UV radiation by ozone. In more recent work, we have developed the capacity to use ozone column information for the specific year of simulation.

The chemical mass balance equations are integrated every hour using a Gear algorithm [*Jacobson and Turco,* 1994] for all grid boxes below the tropopause. The tropopause is diagnosed in the model using the standard criterion of a 2 K km^{-1} lapse rate. Above the tropopause we use a simplified chemical representation which includes production of reactive nitrogen oxides (NO_y) from N_2O oxidation, production of CO and formaldehyde from CH_4 oxidation, and losses of tracers by reaction with OH or photolysis. Stratospheric production rates of NO_y, OH concentration fields, and NO_x/HNO_3 concentration ratios used to partition NO_y are monthly means provided by the 2-D model of *Schneider et al.* [2000]. Photolysis frequencies in the stratosphere are computed with a standard radiative transfer model [*Logan et al.*, 1981]. The resulting cross-tropopause NO_y flux is 0.65 Tg N yr^{-1} (including 0.17 Tg N yr^{-1} as NO_x and 0.48 Tg N yr^{-1} as HNO_3). The main purpose of this simplified stratospheric chemistry is to account for decay of tropospheric tracers transported in the stratosphere, and to provide a source of NO_y to the troposphere. Cross-tropopause transport of ozone produced in the stratosphere requires a special treatment, as described in section 2.5.

2.4. Deposition

Dry deposition of oxidants and water soluble species is computed using a resistance-in-series model based on the original formulation of *Wesely* [1989] with a number of modifications [*Wang et al.*, 1998a]. The dry deposition velocities are calculated locally using GEOS data for surface values of momentum and sensible heat fluxes, temperature, and solar radiation. Wet deposition (applied to HNO_3 and H_2O_2 only) includes scavenging by convective updrafts and anvils and by large-scale precipitation; this algorithm was developed by *Liu et al.* [2001], who evaluated it in the GEOS-CHEM by simulation of the aerosol tracers ^{210}Pb and ^{7}Be.

2.5. Cross-Tropopause Flux of Ozone

Our initial approach to simulate the cross-tropopause ozone flux was to specify ozone concentrations in the lowermost stratosphere (70 hPa) and let the model transport this ozone as an inert tracer into the troposphere. We found that this approach overestimates the flux by a factor of 3-4 with the GEOS-1 data, as diagnosed by the simulation of tropospheric ozone concentrations at high latitudes in winter where transport from the stratosphere is a major source. *Liu et al.* [2001] previously found a similar overestimate in a ^{7}Be simulation with the GEOS-1 fields; they observed that the overestimate is less with the GEOS-STRAT fields but still of a factor 2-3. We have not yet tried this approach with the GEOS-2 or GEOS-Terra fields.

To overcome the difficulty of excessive stratosphere-troposphere exchange in the GEOS-1 and GEOS-STRAT meteorology fields, we have adopted the Synoz (synthetic ozone) method proposed by *McLinden et al.* [2000] to represent cross-tropopause transport of ozone. In this method, stratospheric ozone is represented by a passive tracer that is released uniformly in the tropical lower stratosphere (between 30°S to 30°N and 70 to 10 hPa) at a rate constrained to match a prescribed global mean cross-tropopause ozone flux. We adopted the total flux of 475 Tg O_3 yr^{-1} recommended by *McLinden et al.* [2000] and which results in a satisfactory simulation of vertical ozone profiles at mid and high latitudes in winter, as demonstrated below.

3. Model Evaluation

We present here a general evaluation of the model using a simulation conducted for the year 1994. The simulation uses the GEOS-1 fields degraded from 2°×2.5° horizontal resolution to 4°×5° for the sake of computional expediency; it includes 20 sigma levels in the vertical, from the surface up to 10 hPa with the lowest levels centered at about 50 m, 250 m, 600 m and 1100 m above the surface for a column based at sea level. A 6-month initialization is conducted from July 1, 1993, to January 1, 1994, and we focus our analysis on the 12-month period for 1994.

Simulated ozone concentrations are evaluated by comparison with 1994 and climatological ozonesonde observations [*Logan,* 1999]. CO concentrations are evaluated with aircraft observations as well as surface data from *Novelli et al.* [1998]. Other species simulated in the model including hydrocarbons, acetone, NO, PAN, HNO_3, and H_2O_2 are evaluated through comparison with observations from various aircraft missions that have been averaged over chemically

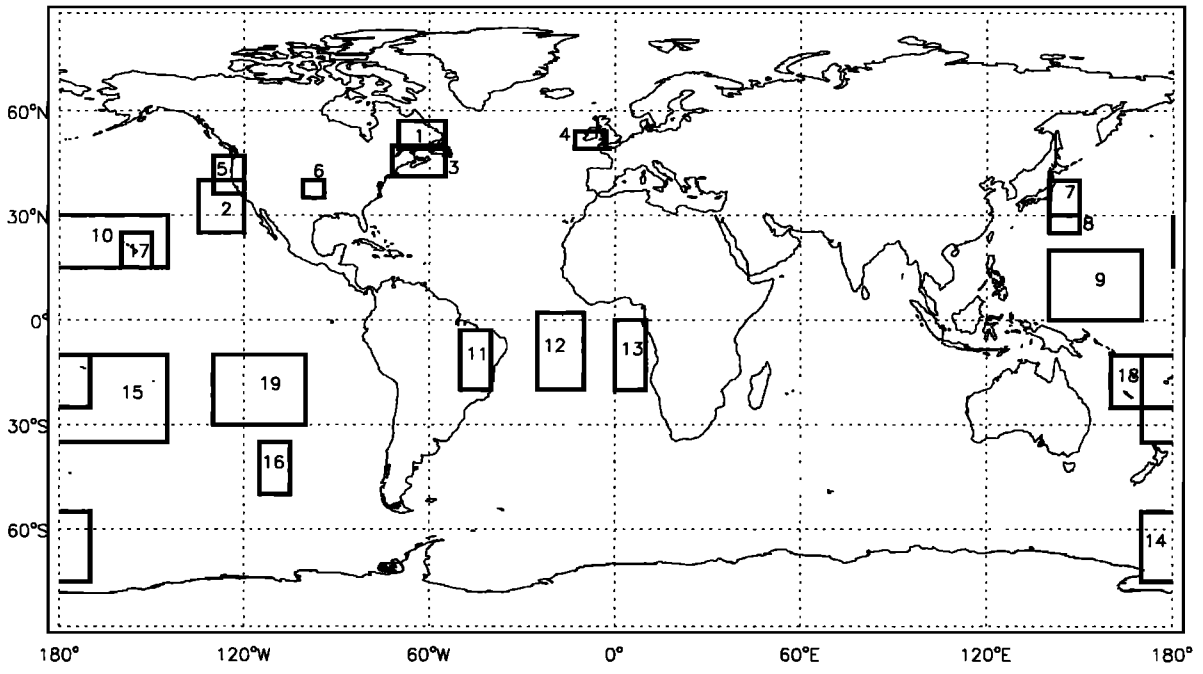

Figure 2. Regions used to aggregate aircraft observations for the purpose of model evaluation. Results are presented for selected regions as listed below. The aircraft mission and the corresponding month used for sampling the model are indicated in parentheses. 1, eastern Canada (July, ABLE 3B); 2, U.S. West Coast (August, CITE 2); 3, Maine (October, SONEX); 4, Ireland (October, SONEX); 5, U.S. West Coast (April, SUCCESS); 6, Kansas (April, SUCCESS); 7, Japan coast (February, PEM-West B); 8, Japan (October, PEM-West A); 9, western Pacific (October, PEM-West A); 10, Hawaii (October, PEM-West A); 11, eastern Brazil (September, TRACE-A); 12, tropical South Atlantic (September, TRACE-A); 13. Africa west coast (September, TRACE-A); 14, Antarctic (September, PEM-Tropics A); 15, tropical South Pacific (September, PEM-Tropics A); 16, south Easter Island (September, PEM-Tropics A); 17, Hawaii (March, PEM-Tropics B); 18, Fiji (March, PEM-Tropics B); 19, Easter Island (March, PEM-Tropics B).

and geographically coherent regions (Figure 2). The regions in Figure 2 are those of *Wang et al.* [1998b] with updates from recent missions (PEM-Tropics A [*Hoell et al.*, 1999], SUCCESS [*Toon and Miakelye*, 1998], SONEX [*Singh et al.*, 1999], and PEM-Tropics B [*Raper et al.*, 2001]) and are similar to those presented in the data compilation of *Emmons et al.* [2000]. The evaluation presented here uses both observations specific to 1994 and statistics of observations for other years. Clearly, the ability to better constrain the evaluation for a specific year is a major advantage of a model driven by assimilated meteorological observations, and the GEOS-CHEM model has been evaluated in other works with such time-specific observations [*Liu et al.*, 2001; *Palmer et al.*, 2001; *Bey et al.*, this issue]. However, observations available for any given year are limited from a global perspective, and interannual variability is sufficiently small that evaluation with observations for other years is still useful for testing the ability of the model to reproduce general features of global distributions of tropospheric ozone and related species.

3.1. Hydroxyl Radical and Hydrogen Peroxide

Figure 3 shows the zonally averaged 24-hour mean OH concentrations simulated by the model for January and July. The distribution of OH is in agreement with current knowledge, i.e. concentrations generally maximum in the tropical midtroposphere (reflecting high UV radiation and water vapor) and in summer at 30°N (reflecting anthropogenic enhancement of NO_x and ozone). The maximum values are higher by 10 to 20% than previous global 3-D models [*Hauglustaine et al.*, 1998; *Wang et al.*, 1998b; *Mickley et al.*, 1999]. The higher OH concentrations relative to our own previous models at Harvard appears to result principally from inclusion in the previous radiative calculations of an absorbing aerosol with optical depth of 0.1 at 310 nm varying inversely with wavelength [*Logan et al.*, 1981]. The degree of UV absorption by tropospheric aerosols, in particular organic aerosols, is highly uncertain. In the present simulation we only include absorption by soot particles with a wavelength-independent optical depth of 0.001.

An evaluation of the global mean OH concentrations simulated by the model can be made using the methylchloroform lifetime as a proxy [*Spivakovsky et al.*, 1990; *Prinn et al.*, 1995]. *Spivakovsky et al.* [2000] derived from observations an atmospheric lifetime of 4.6 years for methylchloroform, in close agreement with *Prinn et al.* [1995]. Assuming stratospheric and ocean sinks for methylchloroform with corresponding lifetimes of 43 and 80 years, respectively, *Spivakovsky et al.* [2000] derived an atmospheric lifetime

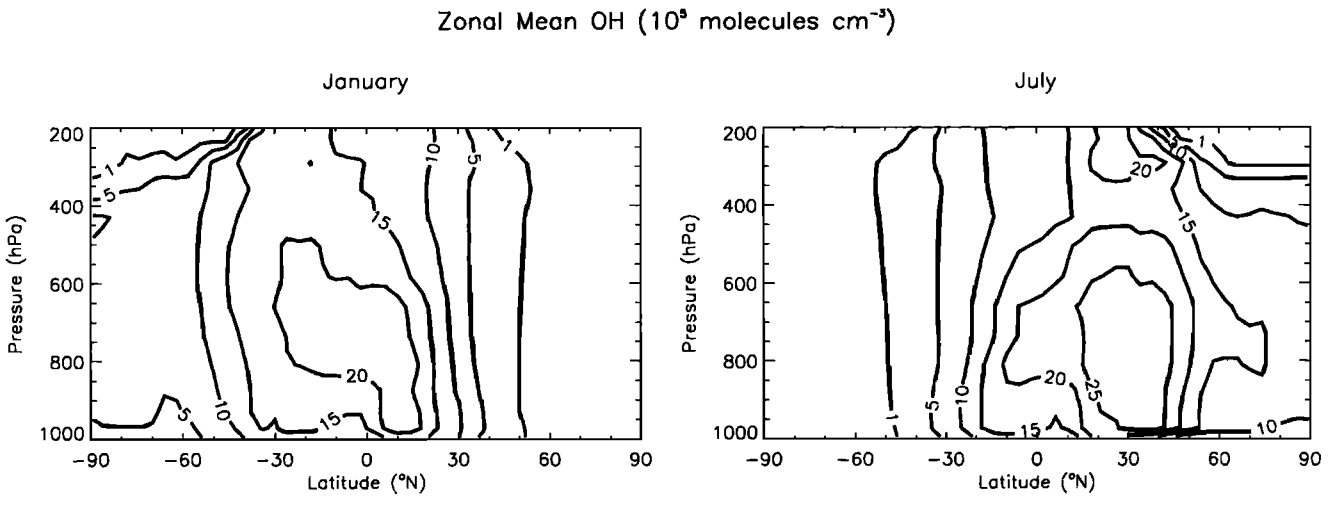

Figure 3. Zonal mean OH concentrations (10^5 molecules cm^{-3}) simulated in the model for January and July.

of methylchloroform against the tropospheric OH sink of 5.5 years. *Wang et al.* [1998b] and *Mickley et al.* [1999] obtained corresponding lifetimes of 6.2 and 7.3 years in their respective models (note that the methylchloroform lifetimes of 5.1 and 6.2 years reported by *Wang et al.* [1998b] and *Mickley et al.* [1999] were calculated considering only the column of methylchloroform up to 200 hPa and 150 hPa, respectively). In our model the atmospheric lifetime against the tropospheric OH sink is 5.1 years. Our value is lower than that of *Spivakovsky et al.* [2000] but is still within the uncertainty of the estimate.

Observations of H_2O_2 allow an additional evaluation of HO_x radical concentrations (HO_x= OH + peroxy radicals) in the model. In most of the troposphere, production of H_2O_2 is the principal sink for HO_x. Figure 4 shows observed vertical profiles of H_2O_2 obtained during several aircraft missions compared to model values for the same geographical region and month. Observed and simulated concentrations both peak at about 2 km, reflecting combined effects of decreasing production with altitude (due to decreasing water vapor) and deposition to the surface. Comparisons for specific regions show significant disagreements, but there is no consistent global bias. The unusually high values observed over Brazil during TRACE-A have been attributed to rapid production in biomass burning plumes [*Lee et al.*, 1997] and are not captured by the model.

3.2. Carbon Monoxide

Simulated monthly mean CO concentrations are compared in Figure 5 with climatological observations in surface air (averaged over 5 to 10 years, depending on the station) as well as observations for 1994. Climatological and 1994 observed values are similar within 10 to 20 ppb except at the Tae-Ahn Peninsula (Korea) where the 1994 data peak at 500 ppb in November while the 6-year mean value peaks only at 300 ppb. The 1994 data for that month consists of only one measurement and can be discarded as anomalous. Observed concentrations are in general higher in the Northern Hemisphere than in the South Hemisphere, reflecting the stronger anthropogenic sources. The wintertime maximum in the Northern Hemisphere reflects in part low concentrations of OH (the main sink of CO) and in part reduced vertical mixing. The spring maximum in the southern tropics (Ascension Island and Samoa) is due to seasonal biomass burning emissions. At most of the sites, simulated CO concentrations exhibit seasonal variations similar to those of observations (with the exception of the peak at Ascension Island, which occurs a month earlier in the model than in the observations). However, at most of the sites the model underestimates CO concentrations by 10 to 20 pbb (and up to 50 ppb). This is seen also in Figure 6 which shows comparison between vertical profiles of observed and simulated CO concentrations: the observed decrease of CO concentrations with altitude in the Northern Hemisphere and the uniform vertical profiles in the Southern Hemisphere are captured by the model, but the simulated concentrations are systematically too low by 10 to 30 ppb.

This problem of CO underestimate was not present in our previous global 3-D models which used similar inventories [*Wang et al.*, 1998b; *Mickley et al.*, 1999]. It arises from higher concentrations of OH in our model, as discussed in section 3.1. In tests we have found that inclusion of an absorbing aerosol in the radiative transfer calculation could correct the CO discrepancy, but there are no good observational constraints for including such an aerosol. In addition, neither our simulation of methylchloroform lifetime nor our calculated H_2O_2 concentrations show any evident bias relative to observations.

The direct CO emissions used in our model are in agreement with the *IPCC* [1995] recommendations but are lower than those used in some other global models: For example, *Hauglustaine et al* [1998] and *Granier et al.* [2000] use a global source of 1218 and 1337 Tg CO yr^{-1}, respectively, while we use a global source of 1043 Tg CO yr^{-1}. The difference is mainly due to natural sources from vegetation and ocean which are poorly known and remain a matter

of speculation. Another uncertain source term for CO is oxidation of NMHC which is estimated by *IPCC* [1995] to be in the range of 200 to 600 Tg CO yr^{-1} but in recent models is reported as 647 Tg CO yr^{-1} [*Granier et al.*, 2000] and 683 Tg CO yr^{-1} [*Holloway et al.*, 2000]. Our CO source from NMHC oxidation of 355 Tg CO yr^{-1} may be too low because the model does not include oxidation of terpenes or higher biogenic hydrocarbons, nor does it include NMHC

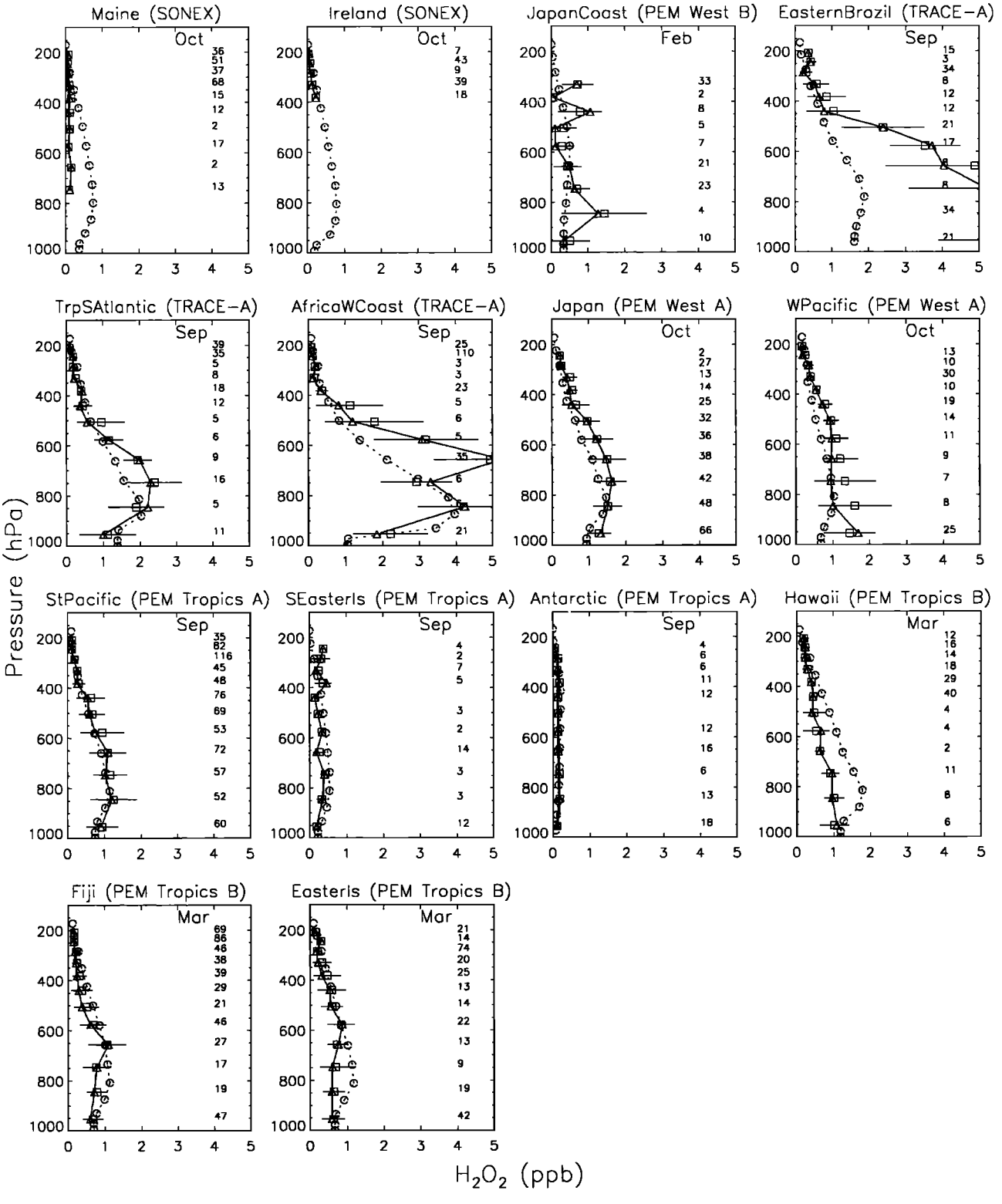

Figure 4. Comparison of observed and simulated vertical profiles of H_2O_2 concentrations. Observations are averaged over the regions in Figure 2. The open squares are mean observed values (with horizontal bars for standard deviations), and the open triangles and solid lines are median observed values. Open circles and dashed lines are simulated values for 1994, sampled over the same region and month.

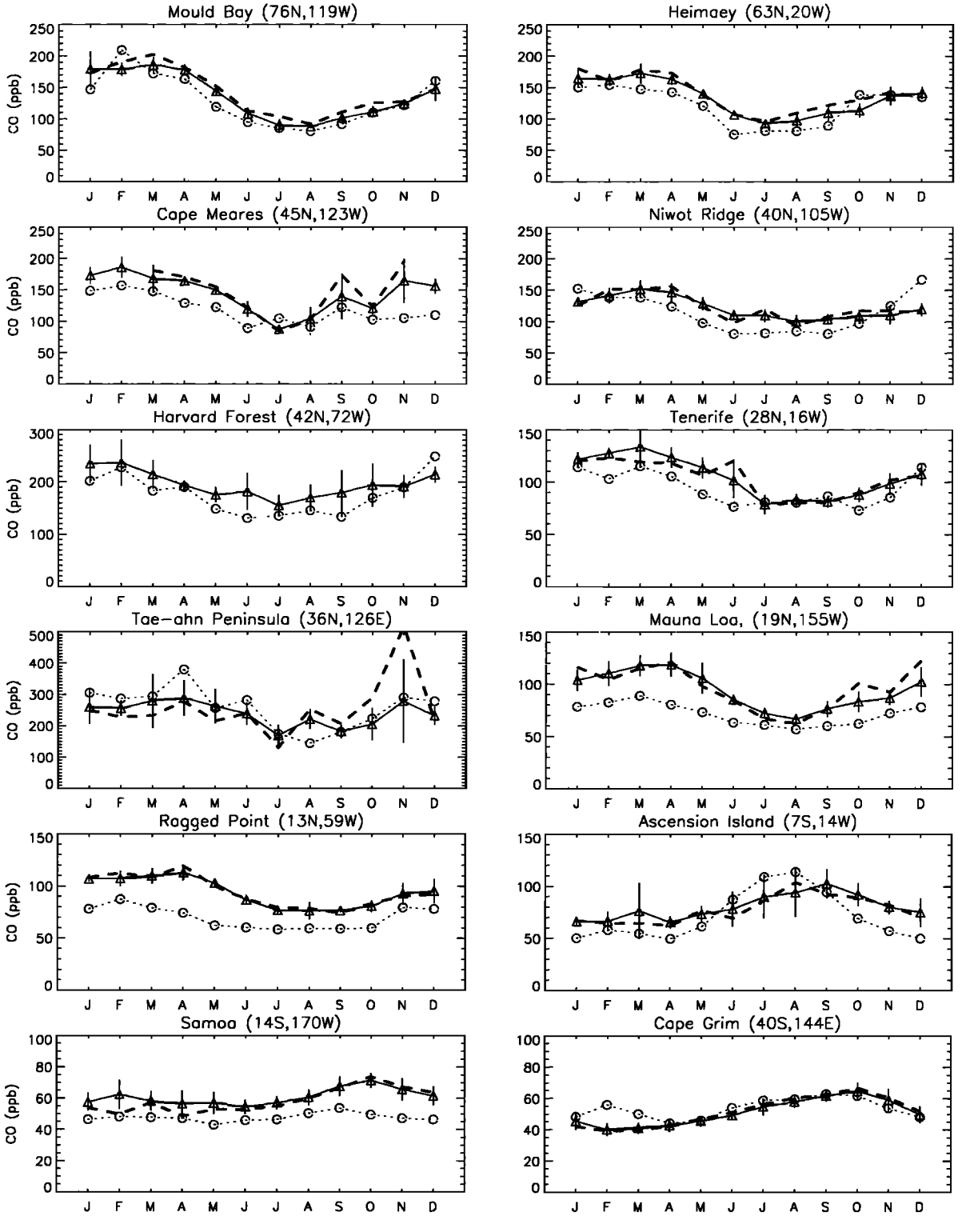

Figure 5. Comparison of observed and simulated monthly mean CO concentrations in surface air. Triangles and solid lines are observed values from *Novelli et al.* [1998] averaged over 5 to 10 years depending on the sites; vertical bars are standard deviations representing interannual variability of the monthly means. Long-dashed lines are the observed values for 1994. Open circles and dashed lines are values from the model for 1994.

emissions from biofuel combustion. Clearly, there are major uncertainties in the sources of CO that could be responsible for our model underestimate of CO concentrations.

3.3. Hydrocarbons and Acetone

Comparison between simulated concentrations and aircraft observations of ethane are shown in Figure 7. Observed ethane concentrations are usually below 500 ppt at remote sites and in the free troposphere and increase in the boundary layer of regions influenced by anthropogenic pollution or biomass burning. The model reproduces the vertical structures but underestimates observed concentrations, by up to a factor 2 in some regions with high anthropogenic emissions (Maine and Japan Coast) and high biomass burning emis-

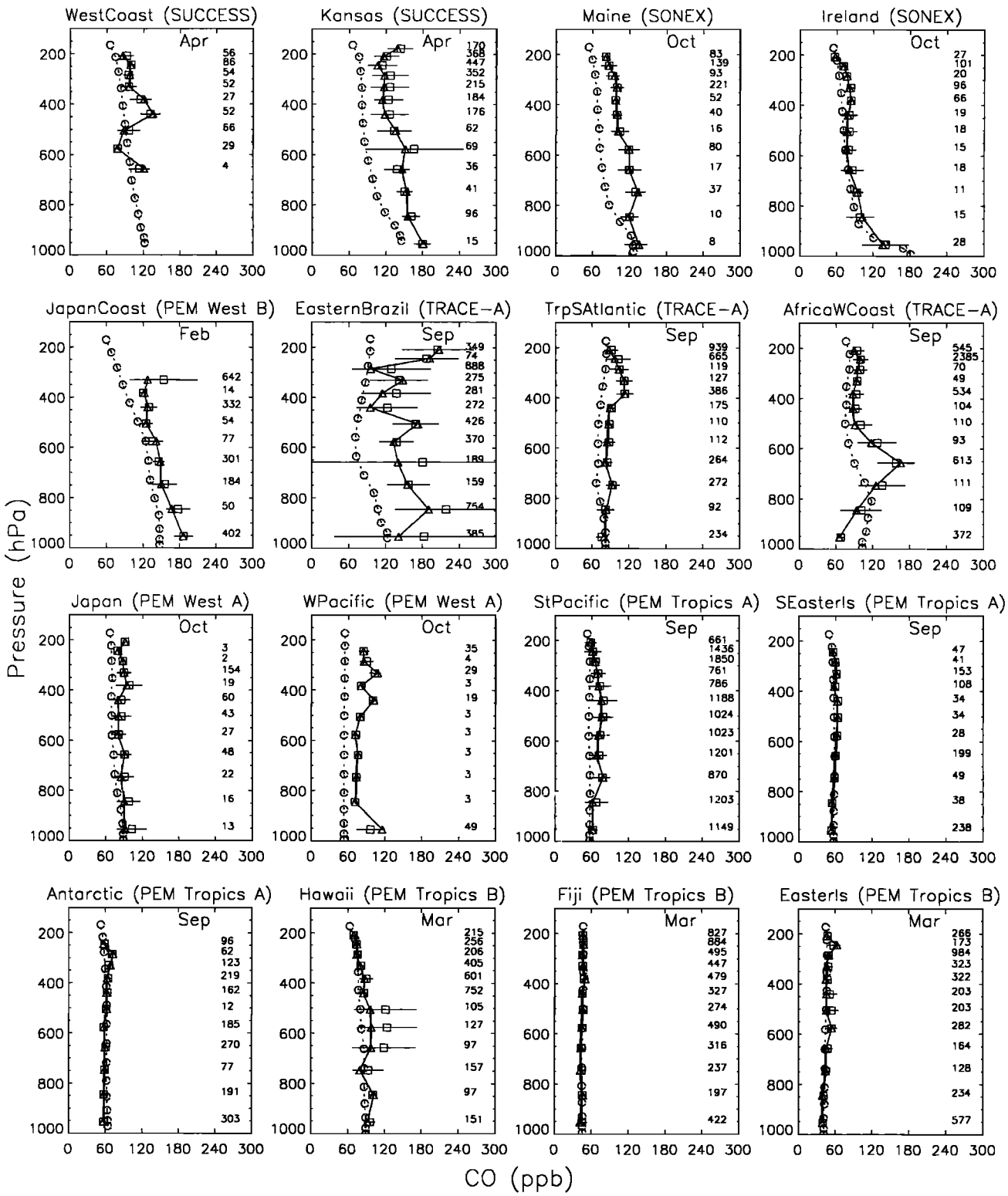

Figure 6. Same as Figure 4, but for CO.

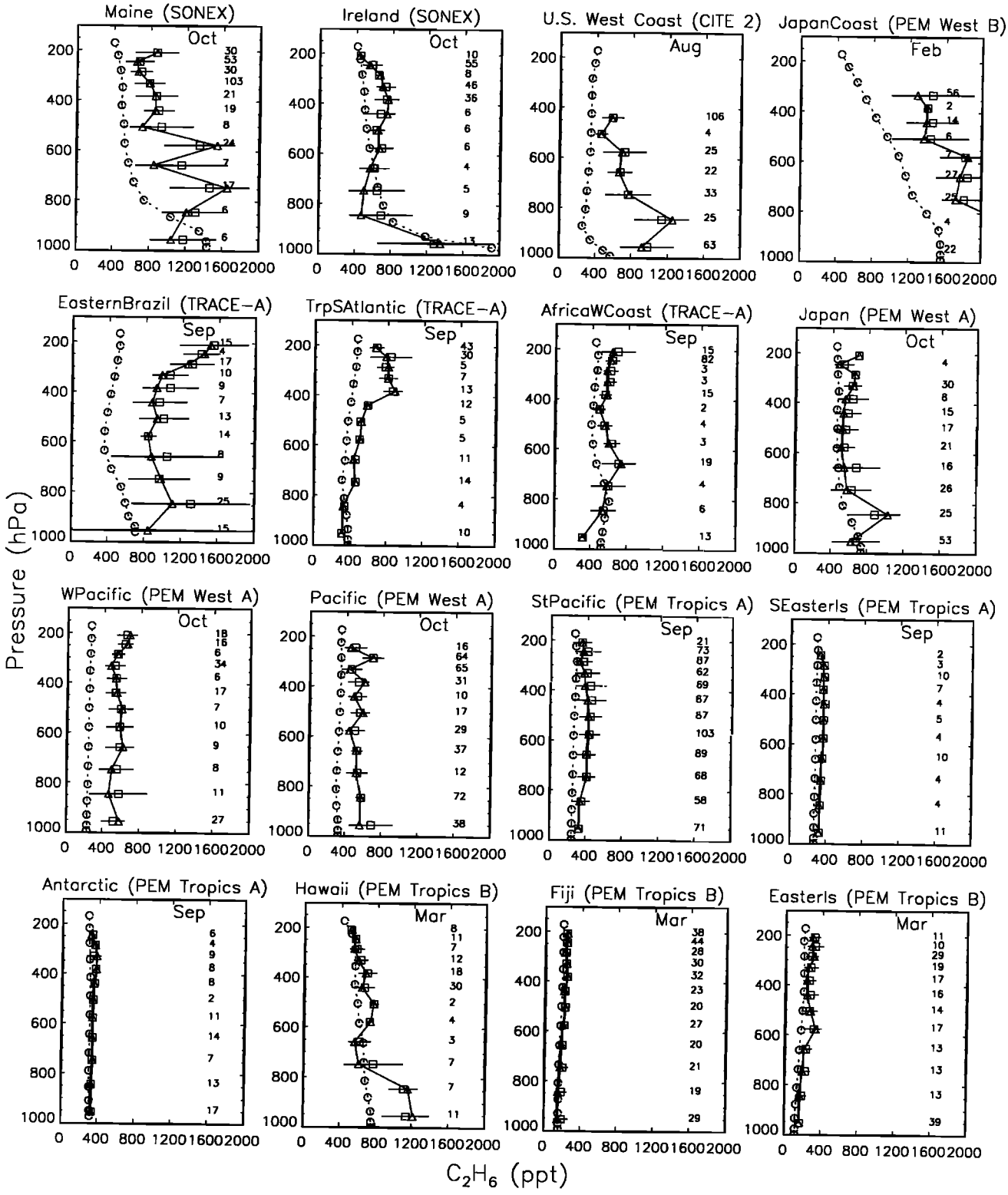

Figure 7. Same as Figure 4, but for ethane.

sions (South Africa and Brazil). A similar underestimate had been previously reported by *Wang et al.* [1998b], thus indicating that this problem is probably not due to our higher OH concentrations but more likely to an underestimate of sources. Model results are too low in regions influenced by both anthropogenic and biomass burning emissions, which points to a possible underestimate of both categories of emissions.

Global ethane sources of *Wang et al.* [1998b] as well as in our model include 6.6 Tg C yr^{-1} from anthropogenic

activities (mainly natural gas) and 3.0 Tg C yr^{-1} from biomass burning. As pointed out by *Wang et al.* [1998b], this global inventory is lower than previous estimates (12-13 Tg C yr^{-1}) from *Rudolph* [1995]. Biogenic and oceanic sources of ethane are not included in our model. These sources appear to be small [*Rudolph,* 1995] but could account for 1.6 Tg C yr^{-1} [*Hauglustaine et al.,* 1998] which would represent a 15% increase of our current total inventory. An underestimate of natural gases emissions in the *Piccot et al.* [1992] inventory is a more likely reason for the underestimate, as found in simulations of propane and isobutane (D. J. Jacob et al., Atmospheric budget of acetone, submitted to Journal of Geophysical Reserach, 2001, hereinafter referred to as Jacob et al., submitted manuscript, 2001).

Figure 8 shows a comparison between simulated monthly means and aircraft observations of isoprene concentrations. Observed values show a strong gradient in the boundary layer, decreasing from about 1 ppb near the surface to less than 0.05 ppb at 3 km at most of the sites. This vertical structure as well as the overall magnitudes of concentrations are captured by the model, lending some support to our estimate of isoprene emission (397 Tg C yr^{-1} globally). The C-shaped profiles simulated over the southeastern United States in summer reflect convective pumping to the middle troposphere, but no observations are available to test this model feature.

Figure 9 compares observed and modeled vertical profiles for acetone. Model results in midlatitudes (Maine and Ireland) agree fairly well with the observations. In eastern Canada, the model underestimates observed values by a factor 2, a problem previously reported by *Wang et al.* [1998b]. Scaling acetone emissions to monoterpene emissions (as is done in the current version of the GEOS-CHEM model) rather than isoprene emissions (as was done in *Wang et al.* [1998a,1998b]) did not correct this underestimate. The model underestimates by a factor of 2-3 observed acetone concentrations over the South Pacific in fall (PEM-Tropics B aircraft mission). Matching these observations would require either a large dispersed secondary source of acetone or a large oceanic emission [*Singh et al.,* 2000b]. An inverse analysis of acetone sources and sinks using the GEOS-CHEM model is presented by D. J. Jacob et al. (submitted manuscript, 2001).

3.4. Nitrogen Species

Comparison of observed and simulated NO and PAN concentrations are shown in Figure 10 and Figure 11. The model typically reproduces NO concentrations within a factor of 2. High NO concentrations over southern Africa and the South Atlantic are due to biomass burning and lightning [*Jacob et al.,* 1996; *Pickering et al.,* 1996]. Lower concentrations are observed elsewhere in the tropics, and again these are well captured by the model. The most severe discrepancy is an overestimate of NO concentrations in the upper troposphere over Hawaii and Fiji during PEM-Tropics B. As discussed

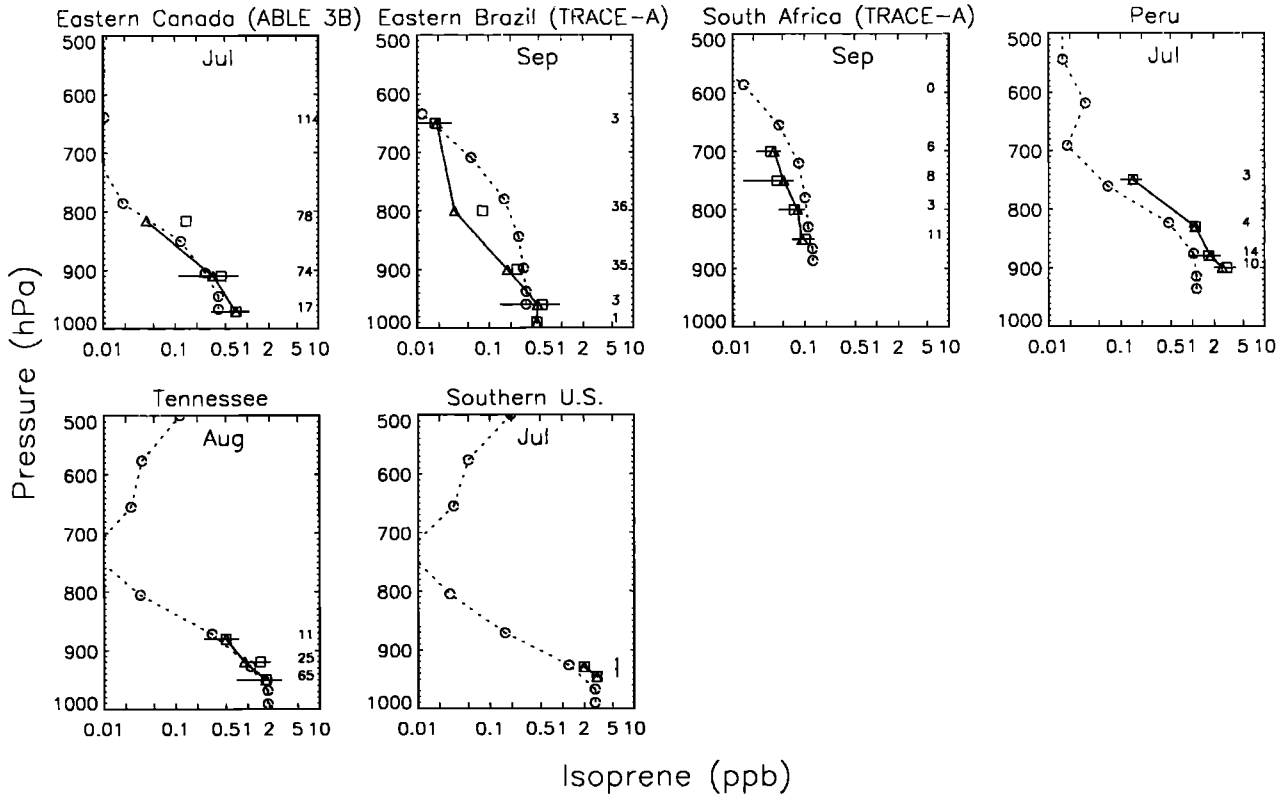

Figure 8. Same as Figure 4, but for isoprene. Data from the "Peru" region are from *Helmig et al.* [1998]; data from the "Tennessee" region are from *Guenther et al.* [1996]; data from the "Southern U.S." region are from *Andronache et al.* [1994].

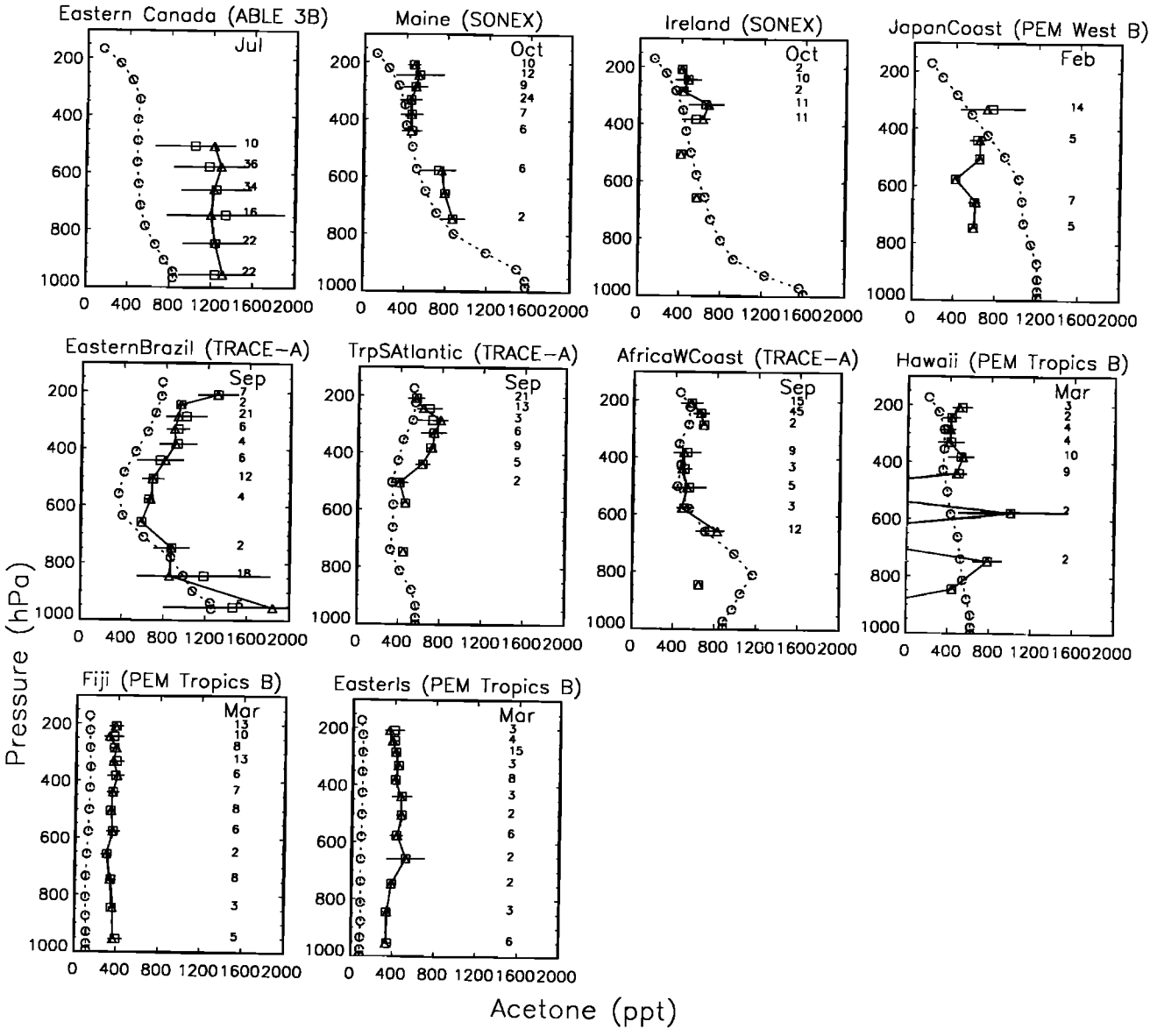

Figure 9. Same as Figure 4, but for acetone.

by *Wang et al.* [2001], these observations were made under conditions of particularly intense marine convection when low-NO_x air from the marine boundary layer is pumped frequently to the upper troposphere.

Peroxyacetylnitrate (PAN) is a reservoir species for NO_x produced by oxidation of organic compounds. Observed PAN concentrations are high over the continental regions (especially where influenced by biomass burning or fossil fuel emissions) and low in regions remote from direct NO_x sources. The model captures similar trends. Simulated concentrations at northern midlatitudes are consistent with observed values although the model overestimates PAN concentrations over Japan in October, a problem previously noted by *Wang et al.* [1998b]. Simulated PAN concentrations for the TRACE-A region, which was heavily impacted by biomass burning, are high but still underestimate observations. Such underestimate was previously noted for ethane and may reflect insufficient NMHC emission from biomass burning in the model.

Nitric acid (HNO_3) is produced in the atmosphere by reaction of NO_2 with OH and by hydrolysis of N_2O_5 in aerosols. Major sinks are dry and wet deposition. Comparison of model results with observed HNO_3 concentrations is shown in Figure 12 . The model typically overestimates the observations by a factor of 2-3. This problem is common to most current global 3-D models of tropospheric chemistry [*Wang et al.*, 1998b; *Hauglustaine et al.*, 1998; *Mickley et al.*, 1999; *Lawrence et al.*, 1999]. The partitioning of HNO_3 into aerosols might provide an explanation since the model does not differentiate between gaseous and aerosol nitrate. There is also strong evidence that the model underestimates precipitation scavenging in the upper troposphere, as shown by *Liu et al.* [2001] in a simulation of ^{210}Pb and ^{7}Be tracers. *Lawrence and Crutzen* [1998] suggested that cirrus precipitation could lead to a considerable scavenging of HNO_3 from the upper troposphere. This process is not represented in our model. (They also suggested that cirrus precipitation would scavenge H_2O_2; however, that seems

dubious since H_2O_2 is only weakly partitioned into the cirrus ice phase [*Mari et al.*, 2000].)

3.5. Ozone

Evaluation of simulated ozone concentrations uses the multiyear climatology of ozonesonde data presented by *Logan* [1999] as well as 1994 ozonesonde measurements. Figure 13 compares simulated and observed seasonal variations of ozone concentrations at 300, 500, and 800 hPa. Where available, 1994 seasonal variations are also reported. The 1994 observations are usually within 20 ppb of the climatology, with the exception of high latitudes at 300 hPa where small shifts in tropopause height can introduce considerable variability in ozone; model evaluation is not

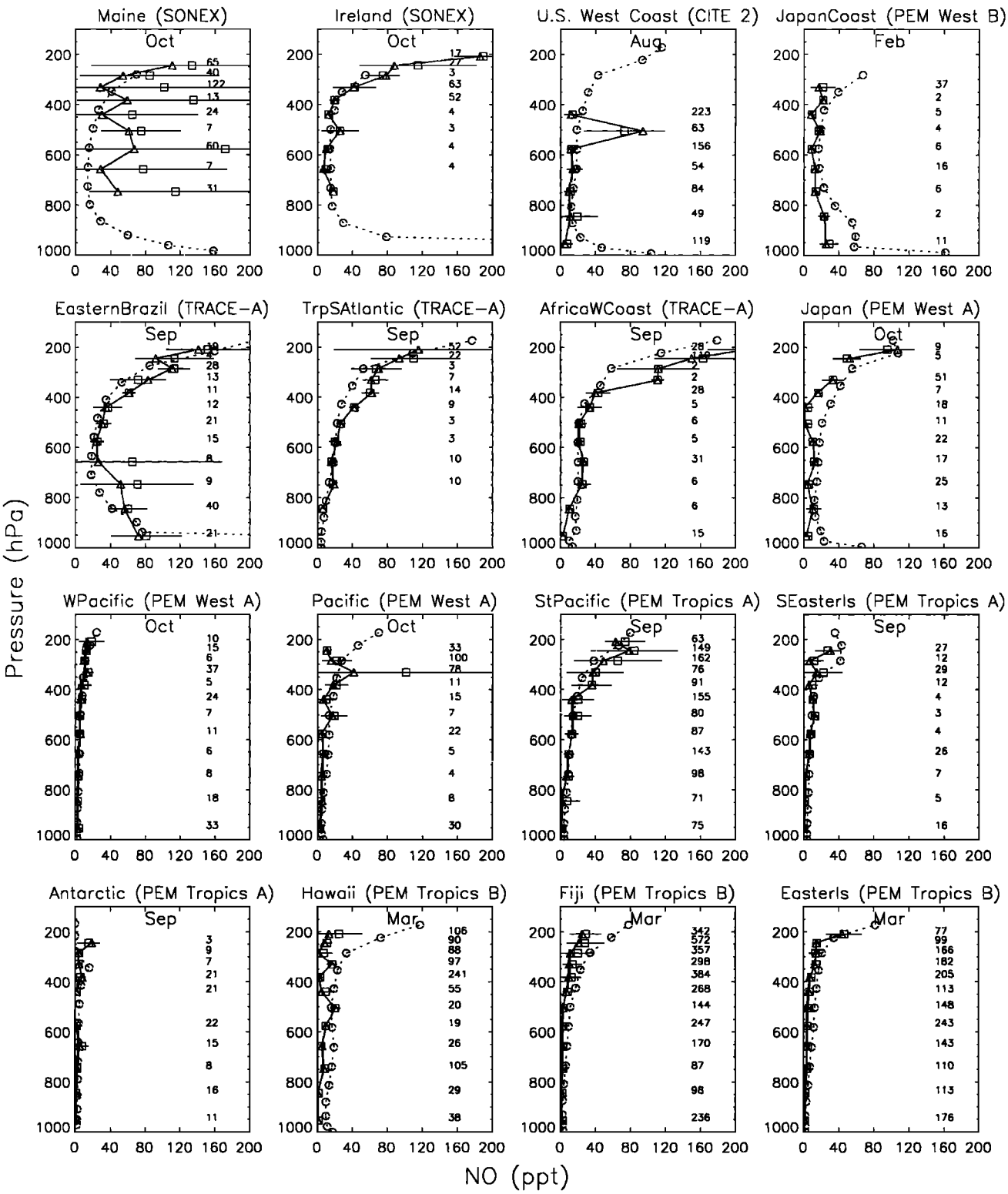

Figure 10. Same as Figure 4, but for NO.

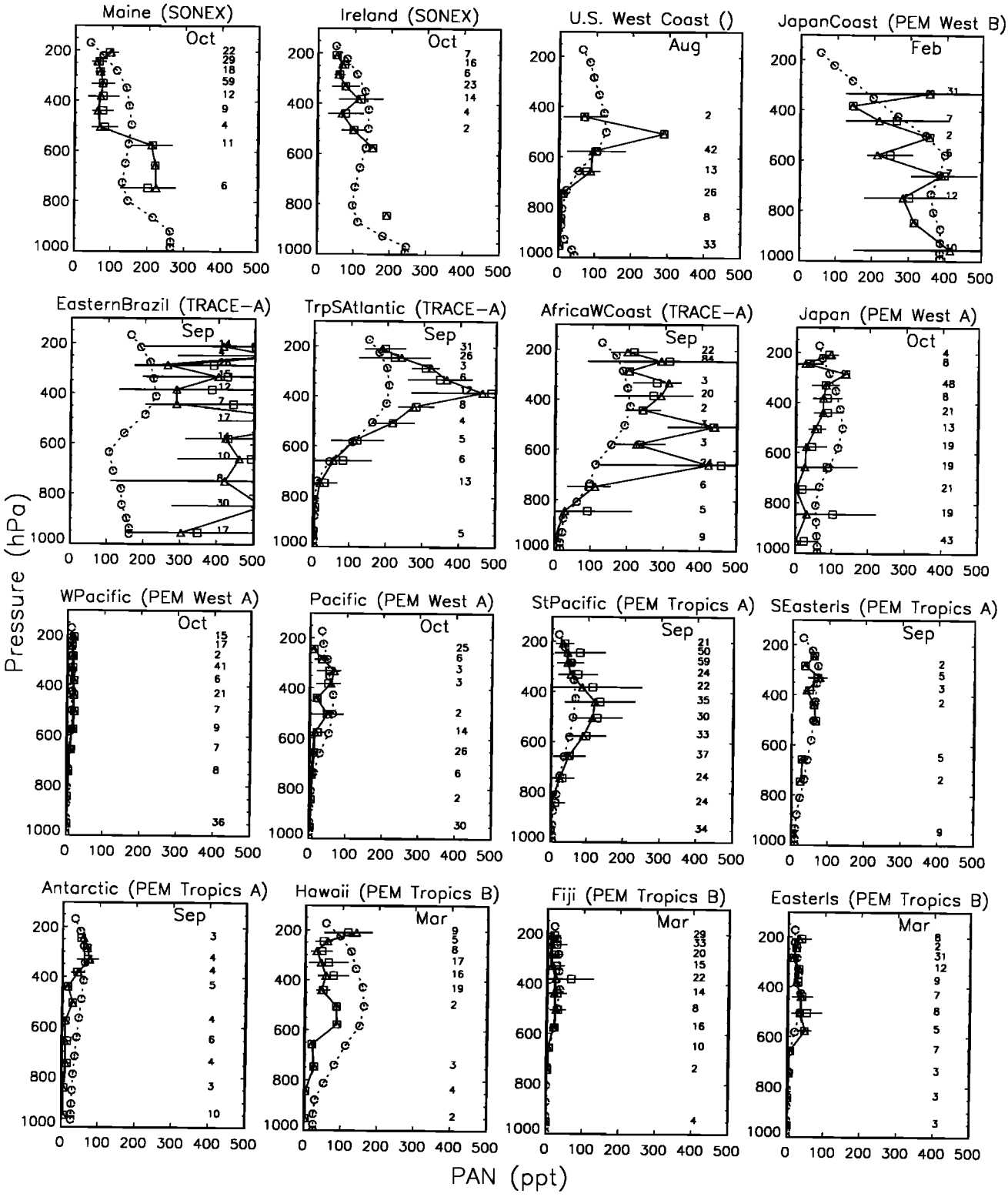

Figure 11. Same as Figure 4, but for PAN.

well constrained at 300 hPa because of this high variability.

The distribution and seasonal variation of tropospheric ozone in the climatology is described in detail by *Logan* [1999]. With a few exceptions, model results are within 10 ppb of the observed values and have the correct seasonal phase. At high northern latitudes the model captures the spring maximum in the lower troposphere and the maximum from May to August in the middle troposphere. Seasonal

variations at northern midlatitudes are relatively well represented. However, the model tends to underestimate slightly the amplitude of the seasonal variation in the extratropics (Hohenpeissenberg and Saporro for example), a problem which we ascribe tentatively to insufficient seasonal variation of cross-tropopause transport (less than that shown by *Wang et al.* [1998a]). Elevated concentrations at 800 hPa at Boulder in summer are likely due to pollution from Denver, which we do not capture well in the model. Good simulation is usually achieved in the tropics and subtropics

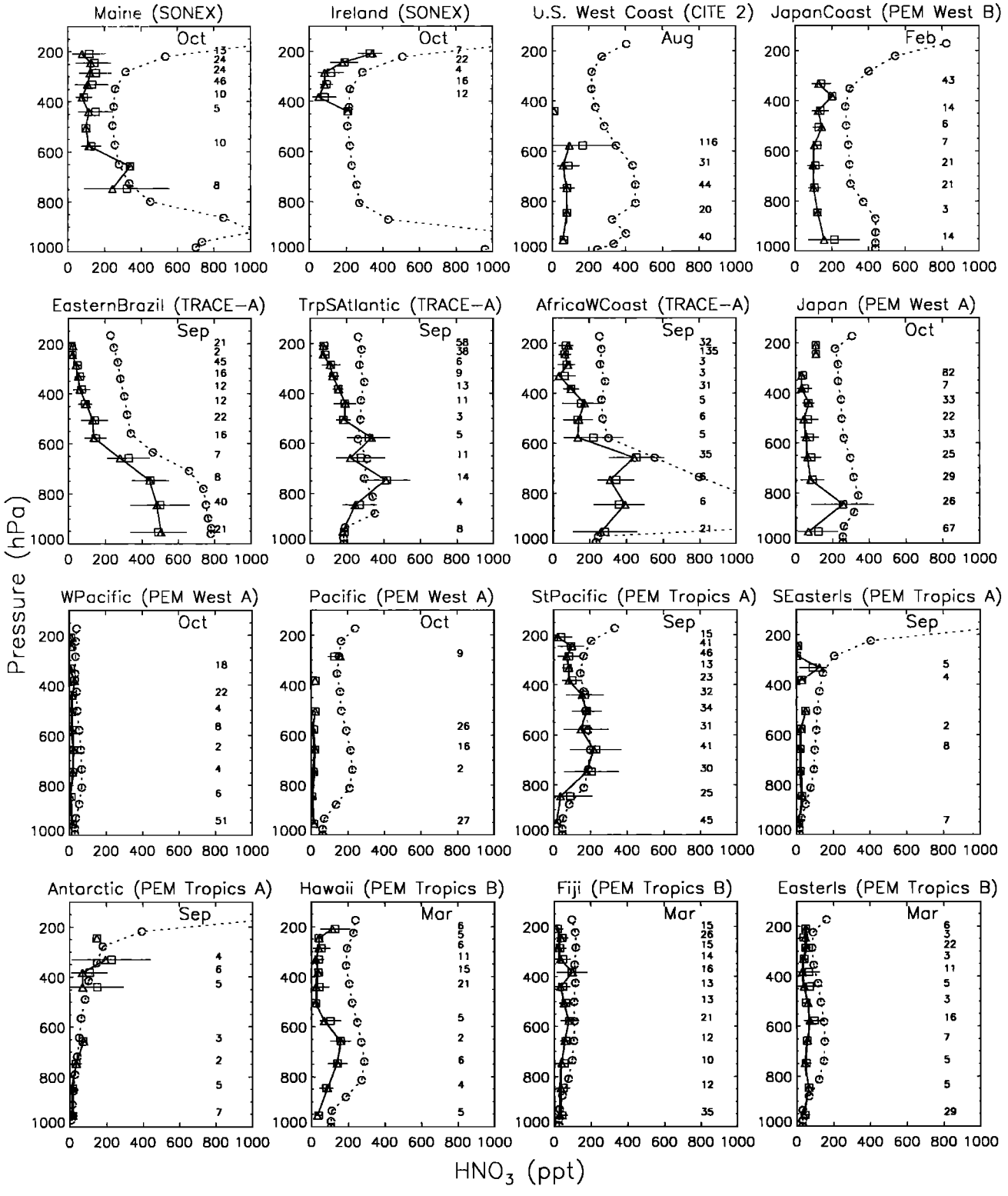

Figure 12. Same as Figure 4, but for HNO_3.

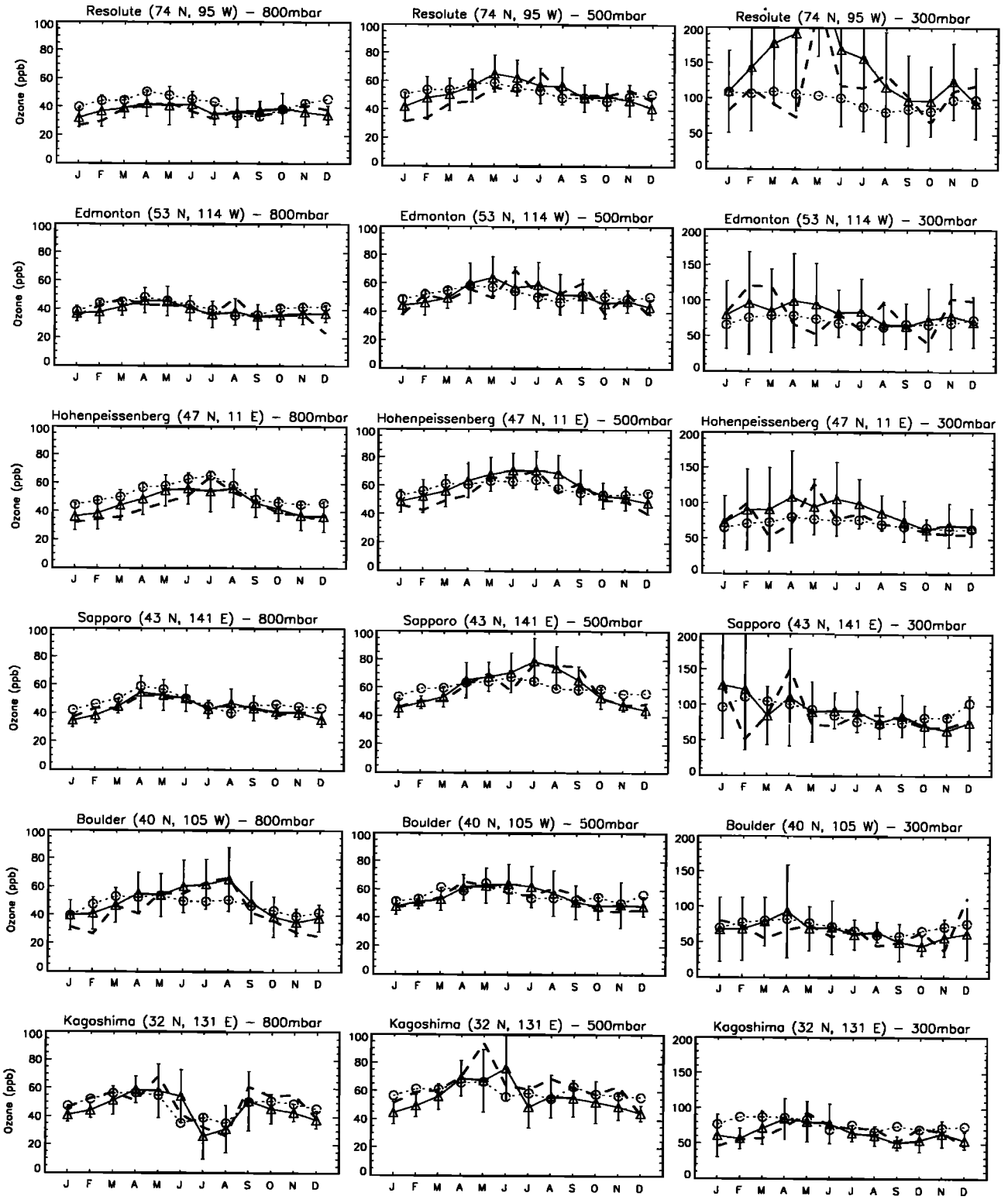

Figure 13. Comparison of observed and simulated monthly mean concentrations of ozone at 800, 500, and 300 hPa. Observations (open triangles and solid lines) are from the ozonesonde climatology of *Logan* [1999]; vertical bars are standard deviations corresponding to interannual variability. Long-dashed lines are the observed values for 1994 (there are no observations in 1994 at Samoa and Natal). Model values (open circles and dashed lines) are for 1994.

to within the constraints offered by the observations. The observed minima in eastern Asia (Kagoshima and Naha) due to the summer monsoon are captured by the model. The spring maximum and summer minimum observed in the northern subtropics (Hilo, for example) are well represented by the model throughout the troposphere. Observations in the southern tropics (Natal) show a large austral spring maximum due to biomass burning emissions that the model captures well. The longitudinal gradient observed in the southern tropics between Natal and Samoa is also well captured.

Table 5 gives the global budget of tropospheric ozone in the model. The global photochemical production and destruction rates of ozone are 4900 Tg yr^{-1} and 4300 Tg

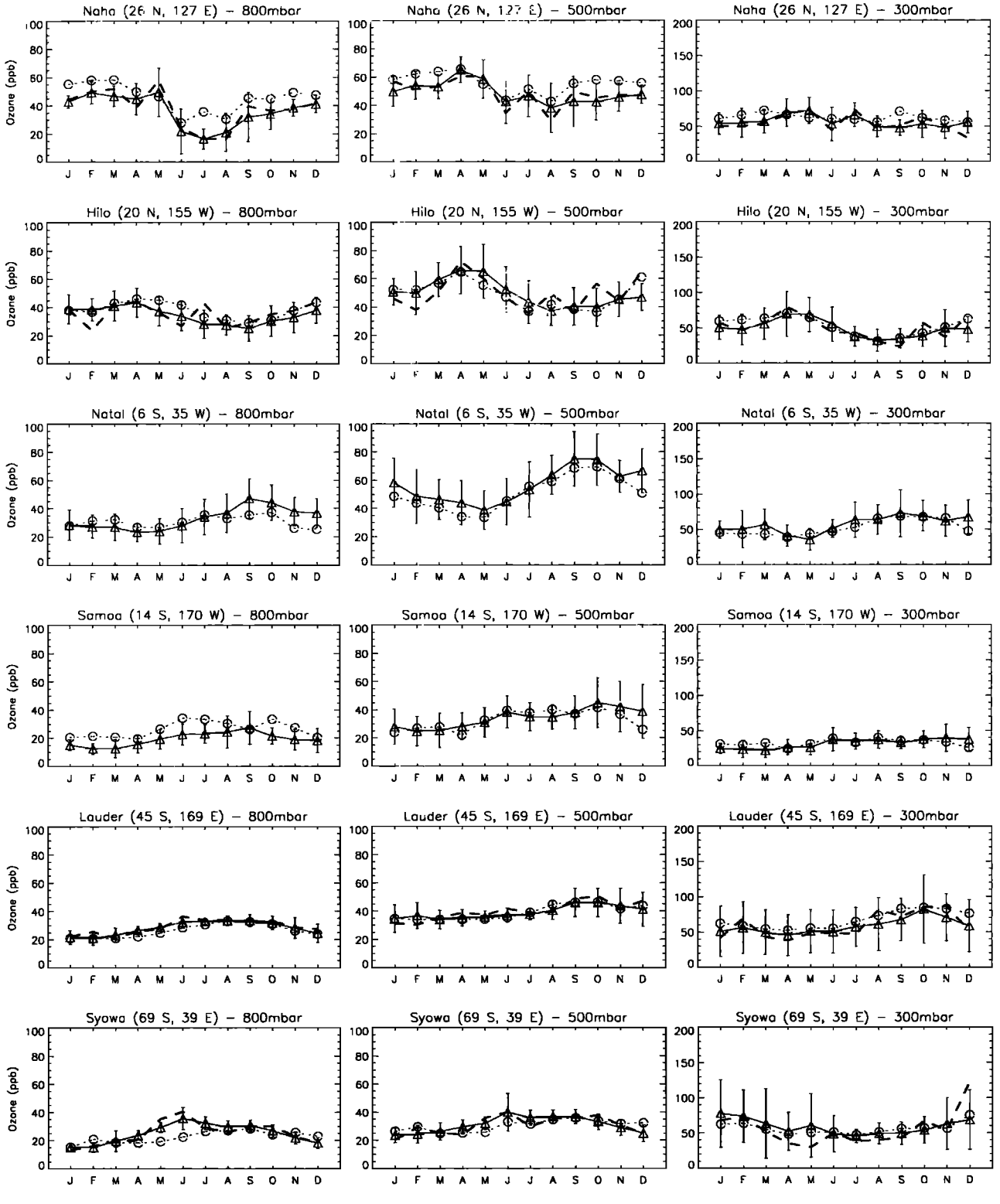

Figure 13. (continued)

Table 5. Global Budget for Tropospheric Ozone in the GEOS-CHEM Model

	Global	Northern Hemisphere	Southern Hemisphere
Sources, Tg O_3 yr^{-1}			
Chemical production	4900	3100	1800
Stratospheric influx	470	280	190
Total	5370	3380	1990
Sinks, Tg O_3 yr^{-1}			
Chemical loss	4300	2600	1700
Deposition	1070	740	330
Total	5370	3340	2030
Burden, Tg O_3	315	175	140

The budget is for the extended odd oxygen family defined as O_3 + NO_2 +2×NO_3 + PAN + PPN + MPAN + HNO_4 + HNO_3 + 3×N_2O_5 and applies to the column up to the model tropopause. Values are annual means for 1994.

yr^{-1}, respectively, with a stratospheric input of 470 Tg yr^{-1}. Previous global 3-D models indicate photochemical production ranging from 3314 to 4550 Tg yr^{-1} and photochemical loss ranging from 2511 to 4065 Tg yr^{-1} [*WMO*, 1998; *Lelieveld and Dentener*, 2000]. Stratospheric inputs in these models vary from 390 to 768 Tg yr^{-1} [*WMO*, 1998]. Our calculated values for the photochemical terms are at the high end of previous models. They are in particular higher than in our previous global 3-D models at Harvard; *Mickley et al.* [1999] and *Wang et al.* [1998b] report production rates of 4330 and 4100 Tg yr^{-1} and loss rates of 3960 and 3680 Tg yr^{-1}, respectively. The difference appears to reflect the stronger UV actinic fluxes in the present model, as discussed previously.

4. Conclusion

This paper provided a first description of GEOS-CHEM, a global 3-D model of tropospheric chemistry driven by GEOS assimilated meteorological fields from the NASA Data Assimilation Office (DAO). A 1-year simulation is presented for 1994, and results are evaluated with observations both for 1994 and for other years. We show that the model is capable of representing the general features of the global distributions of tropospheric ozone and related species although there are some significant discrepancies.

Global chemical production and loss rates of tropospheric ozone, as well as global OH concentrations, are at the high end of values previously reported in global 3-D models including earlier generations of our 3-D model at Harvard. This difference appears largely due to our suppression of an UV-absorbing background aerosol (with an optical depth of 0.1 at 310 nm) that was present in the earlier models. Although organic aerosols in the troposphere are expected to absorb UV radiation, there are no observations available to usefully constrain the corresponding optical depth at the wavelengths of interest. The present model can accommodate the observed methylchloroform lifetime and H_2O_2 concentrations (which provide standard tests of photochemical activity for global models) within the constrains provided by these observations. However, that does not exclude model OH for possibly being too high by ~20%.

The model systematically underestimates observed CO concentrations by 10-30 ppb, which could reflect a problem with current source inventories as well as an overestimate of OH. Simulation of ethane indicates an underestimate of sources. The large underestimate of acetone concentrations over the South Pacific suggests a large oceanic source. Simulated concentrations of NO and PAN are generally within a factor of 2 of observed values (often much better) and show the correct vertical structure. The model overestimates HNO_3 concentrations by factors of 2-3 in the remote troposphere, a problem which we attribute in part to insufficient scavenging.

The model reproduces well the global distribution of tropospheric ozone concentrations as determined from ozonesonde observations. It simulates usually to within 10 ppb the 1994 observations as well as the multiyear climatology (which are similar except near the tropopause). It captures the observed seasonal phases and amplitudes in different regions of the troposphere. There is a slight underestimate in the amplitude of the seasonal variation in the extratropical Northern Hemisphere which we attribute to insufficient seasonal variation in the parameterized cross-tropopause ozone flux.

In a companion paper [*Bey et al.*, this issue], we use the GEOS-CHEM model to examine the Asian outflow of ozone, CO, and NO_y species over the western Pacific by simulation of observations from the PEM-West B aircraft mission in February-March 1994.

Acknowledgments. This research was supported by the NASA Atmospheric Chemistry Modeling and Analysis Program (ACMAP) and by the NASA Earth Observing System (EOS). We wish to thank Clarissa Spivakovsky for very helpful discussions. We are grateful to Andrew Fusco for processing isoprene observations.

References

Adams, P.J., J.H. Seinfeld, D. Koch, L.J. Mickley, and D.J. Jacob, General circulation model assessment of direct radiative forcing by the sulfate-nitrate-ammonium-water inorganic aerosol system, *J. Geophys. Res., 106*, 1097-1111, 2001.

Allen, D.J., R.B. Rood, A.M. Thompson, and R.D. Hidson, Three-dimensional ^{222}Rn calculations using assimilated data and a

convective mixing algorithm, *J. Geophys. Res., 101,* 6871-6881, 1996a.

Allen, D.J., et al., Transport induced interannual variability of carbon monoxide using a chemistry and transport model, *J. Geophys. Res., 101,* 28,655-28,670, 1996b.

Andronache, C., W.L. Chameides, M.O. Rodgers, J. Martinez, P. Zimmerman, and J. Greenberg, Vertical distribution of isoprene in the lower boundary layer of the rural and urban southern United States, *J. Geophys. Res., 99,* 16,989-16,999, 1994.

Atkinson, R., Gas-phase tropospheric chemistry of volatile organic compounds, 1, Alkanes and alkenes, *J. Phys. Chem. Ref. Data, 26,* 215-290, 1997.

Benkovitz, C.M., M.T Schultz, J. Pacyna, L. Tarrason, J. Dignon, E.C. Voldner, P.A. Spiro, J.A. Logan, and T.E. Graedel, Global gridded inventories for anthropogenic emissions of sulfur and nitrogen, *J. Geophys. Res., 101,* 29,239-29,253, 1996.

Bey, I., D.J. Jacob, J.A. Logan, and B. Yantosca, Asian chemical outflow to the Pacific in spring: Origins, pathways, and budgets, *J. Geophys. Res.,* this issue.

Brasseur, G.P., D.A. Hauglustaine, S. Walters, P.J. Rasch, J.F. Müller, C. Granier, and X.X. Tie, MOZART, A global chemical transport model for ozone and related chemical tracers, 1, Model description, *J. Geophys. Res., 103,* 28,265-28,289, 1998.

Brown, S.S., R.K. Talukdar, and A.R. Ravishankara, Rate constant for the reaction $OH+NO_2+M \rightarrow HNO_3+M$ under atmospheric conditions, *Chem. Phys. Lett., 299,* 277-284, 1999a.

Brown, S.S., R.K. Talukdar, and A.R. Ravishankara, Reconsideration of the rate constants for the reaction of hydroxyl radicals with nitric acid vapor, *J. Phys. Chem., 103,* 3031-3037, 1999b.

Chen, X.H., D. Hulbert, P.B. Shepson, Measurement of the organic nitrate yield from OH reaction with isoprene, *J. Geophys. Res., 103,* 25,563-25,568, 1998.

Chin, M., D.J. Jacob, G.M. Gardner, M.S. Foreman-Fowler, P.A. Spiro, and D.L. Savoie, A global three-dimensional model of tropospheric sulfate, *J. Geophys. Res., 101,* 18,667-18,690, 1996.

Collins, W.J., D.S. Stevenson, C.E. Johnson, and R.G. Derwent, Tropospheric ozone in a global-scale three-dimensional lagrangian model and its response to NO_x emission controls, *J. Atmos. Chem., 26,* 223-274, 1997.

DeMore, W.B., S.P. Sander, D.M. Golden, R.F. Hampson, M.J Kurylo, C. J. Howard, A. R. Ravishankara, C.E. Kolb, and M.J. Molina, Chemical kinetics and photochemical data for use in stratospheric modeling, *JPL Publ., 97-4,* 1997.

European Monitoring and Evaluation Programme (EMEP), Transboundary air pollution in Europe, part 1, Emissions, dispersion and trends of acidifying and eutrophying agents, *EMEP/MSC-W Rep. 1/97,* Norw. Meteorol. Inst., Oslo, Norway, 1997.

Emmons, L.K., D.A. Hauglustaine, J.F. Müller, M.A. Carroll, G.P. Brasseur, D. Brunner, J. Staehelin, V. Thouret, and A. Marenco, Data composites of airborne observations of tropospheric ozone and its precursors, *J. Geophys. Res., 105,* 20497-20538, 2000.

Environmental Protection Agency (EPA), National air pollutant emission trends, 1990-1996, *Rep. EPA-454/R-97-011,* Research Triangle Park, N.C., 1997.

Flatoy, F., O. Hov, and H. Schlager, Chemical forecasts used for measurement flight planning during POLINAT 2, *Geophys. Res. Lett., 27,* 951-954, 2000.

Granier, C., G. Petron, J.-F. Müller, and G. Brasseur, The impact of natural and anthropogenic hydrocarbons on the tropospheric budget of carbon monoxide, *Atmos. Environ., 34,* 5255-5270, 2000.

Guenther, A., et al., A global model of natural volatile organic compound emissions, *J. Geophys. Res., 100,* 8873-8892, 1995.

Guenther, A., et al., Isoprene fluxes measured by enclosure, relaxed eddy accumulation, surface layer gradient, mixed layer gradient, and mixed layer mass balance techniques, *J. Geophys. Res., 101,* 18,555-18,567, 1996.

Hansen, J., G. Russell, D. Rind, P. Stone, A. Lacis, S. Lebedeff, R. Ruedy, and L. Travis, Efficient three-dimensional models for climate studies: Models I and II, *Mon. Weather Rev., 3,* 609–662, 1983.

Hauglustaine, D.A., G.P. Brasseur, S. Walters, P.J. Rasch, J.F. Müller, L.K. Emmons, and M.A. Carroll, MOZART: A global chemical transport model for ozone and related chemical tracers, 2, Model results and evaluation, *J. Geophys. Res., 103,* 28,291-28,335, 1998.

Helmig, D., et al., Vertical profiling and determination of landscape fluxes of biogenic nonmethanes hydrocarbons within the planetary boundary layer in the Peruvian Amazon, *J. Geophys. Res., 103,* 25,519-25,532, 1998.

Hoell, J.M., D.D. Davis, S.C. Liu, R.E. Newell, M. Shipham, H. Akimoto, R.J. McNeal, R.J. Bendura, and J.W. Drewry, Pacific Exploratory Mission West-A (PEM West-A): September-October 1991, *J. Geophys. Res., 101,* 1641-1653, 1996.

Hoell, J.M., et al., Pacific Exploratory Mission-West Phase B: February-March 1994, *J. Geophys. Res., 102,* 28,223-28,240, 1997.

Hoell, J.M., D.D. Davis, D.J. Jacob, M.O. Rodgers, R.E. Newell, H.E. Fuelberg, R.J. McNeal, J.L. Raper, and R.J. Bendura, The Pacific Exploratory Mission in the tropical Pacific: PEM-Tropics A, August-September 1996, *J. Geophys. Res., 104,* 5567-5584, 1999.

Holloway, T., H. Levy II, and P. Kasibhatla, Global distribution of carbon monoxide, *J. Geophys. Res., 105,* 12,123-12,147, 2000.

Horowitz, L.W., and D.J. Jacob, Global impact of fossil fuel combustion on atmospheric NO_x *J. Geophys. Res., 104,* 23,823-23,840, 1999.

Horowitz, L.W., J. Liang, G.M. Gardner, and D.J. Jacob, Export of reactive nitrogen from North America during summertime: Sensitivity to hydrocarbon chemistry, *J. Geophys. Res., 103,* 13,451-13,476, 1998.

Intergovernmental Panel on Climate Change (IPCC), Radiative forcing of climate change and an evaluation of the IPCC IS92 emission scenarios, in *Climate Change 1994: The Science of Climate Change,* edited by J.T. Houghton et al., Cambridge Univ. Press, New York, 1995.

Intergovernmental Panel on Climate Change (IPCC), Atmospheric chemistry and greenhouse gases, in *Climate Change 2001: The Scientific Basis,* edited by J.T. Houghton et al., Cambridge Univ. Press, New York, 2001.

Jacob, D.J., Heterogeneous chemistry and tropospheric ozone, *Atmos. Environ., 34,* 2131-2159, 2000.

Jacob, D.J., et al., Evaluation and intercomparison of global atmospheric transport models using radon-222 and other short-lived tracers, *J. Geophys. Res., 102,* 5953-5970, 1997.

Jacob, D.J., et al., Origin of ozone and NO_x in the tropical troposphere: A photochemical analysis of aircraft observations over the South Atlantic Basin, *J. Geophys. Res., 101,* 24,235-24,250, 1996.

Jacobson, M.Z., and R.P. Turco, A sparse-matrix, vectorized GEAR code for atmospheric transport models, *Atmos. Environ., 33,* 273-284, 1994.

Kanakidou, M., et al., 3D global simulations of tropospheric CO distributions - Results of the GIM/IGAC intercomparison 1997 exercise, *Chemosphere Global Change Sci., 1,* 263-282, 1999.

Klinger, L.F., J. Greenberg, A. Guenther, G. Tyndall, P. Zimmerman, M. M'Bangui, J.M. Moutsambot, and D. Kenfck, Patterns in volatile organic compound emissions along a savanna-rainforest gradient in central Africa, *J. Geophys. Res., 103,* 1443-1454, 1998.

Lawrence, M.G., and P.J. Crutzen, The impact of cloud particle gravitational settling on soluble trace gas distributions, *Tellus, 50,* 263-289, 1998.

Lawrence, M.G., P.J. Crutzen, P.J. Rasch, B.E. Eaton, and N.M. Mahowald, A model for studies of tropospheric photochemistry: Description, global distributions, and evaluation, *J. Geophys. Res., 104,* 26,245-26,277, 1999.

Lee, M., B. G. Heikes, D.J. Jacob, G. Sachse, and B. Anderson, Hydrogen peroxide, organic hydroperoxide, and formaldehyde

as primary pollutants from biomass burning, *J. Geophys. Res., 102*, 1301-1309, 1997.

Levy, H., W.J. Moxim, A.A. Klonecki, and P.S. Kasibhatla, Simulated tropospheric NO_x: Its evaluation, global distribution, and individual source contributions, *J. Geophys. Res., 104*, 26,279-26,306, 1999.

Lelieveld, J., and F.J. Dentener, What controls tropospheric ozone?, *J. Geophys. Res., 105*, 3531-3551, 2000.

Li, Q., D.J. Jacob, I. Bey, R.M. Yantosca, Y. Zhao, Y. Kondo, and J. Notholt, Atmospheric hydrogen cyanide (HCN): Biomass burning source, ocean sink? *Geophys. Res. Lett., 27*, 357-360, 2000.

Liang, J., L.W. Horowitz, D.J. Jacob, Y. Wang, A.M. Fiore, J.A. Logan, G.M. Gardner, and J.W. Munger, Seasonal budgets of reactive nitrogen species and ozone over the United States, and export fluxes to the global atmosphere, *J. Geophys. Res., 103*, 13,435-13,450, 1998.

Lin, S.-J., and R. B. Rood, Multidimensional flux form semi-Lagrangian transport schemes, *Mon. Weather Rev., 124*, 2046-2070, 1996.

Liu, H., D.J. Jacob, I. Bey, and R.M. Yantosca, Constraints from ^{210}Pb and ^{7}Be on wet deposition and transport in a global three-dimensional chemical tracer model driven by assimilated meteorological fields, *J. Geophys. Res., 106*, 12,109-12,128, 2001.

Logan, J.A., An analysis of ozondesonde data for the troposphere: Recommendations for testing 3-D models and development of a gridded climatology for tropospheric ozone, *J. Geophys. Res., 104*, 16,115–16,149, 1999.

Logan, J.A., M.J. Prather, S.C. Wofsy, and M.B. McElroy, Tropospheric chemistry: A global perspective, *J. Geophys. Res., 86*, 7210-7254, 1981.

Mari, C., D.J. Jacob, and P. Bechtold, Transport and scavenging of soluble gases in a deep convective cloud, *J. Geophys. Res., 105*, 22,255-22,267, 2000.

Marland, G., T.A. Boden, R. J. Andres, A. L. Brenkert, and C. A. Johnston, Global, regional, and national fossil fuel CO_2 emissions, In *Trends: A Compendium of Data on Global Change*, Carbon Dioxide Inf. Anal. Cent., Oak Ridge Nat. Lab., U.S. Dep. of Energy, Oak Ridge, Tenn., 1999.

McLinden, C.A., S.C. Olsen, B. Hannegan, O. Wild, M.J. Prather, and J. Sundet, Stratospheric ozone in 3-D models: A simple chemistry and the cross-tropopause flux, *J. Geophys. Res., 105*, 14,653-14,665, 2000.

Mickley, L.J., P.P. Murti, D.J. Jacob, J.A. Logan, D. Rind, and D. Koch, Radiative forcing from tropospheric ozone calculated with a unified chemistry-climate model, *J. Geophys. Res., 104*, 30,153-30,172, 1999.

Middleton, P., W.R. Stockwell, and W.P.L. Carter, Aggregation and analysis of volatile organic compounds emissions for regional modeling, *Atmos. Environ., 24*, 1107-1133, 1990.

Novelli, P.C., K.A. Masarie, and P.M. Lang., Distributions and recent changes in carbon monoxide in the lower troposphere, *J. Geophys. Res., 103*, 19,015-19,033, 1998.

Palmer, P.I., D.J. Jacob, K. Chance, R.V. Martin, R.J.D. Spurr, T.P. Kurosu, I. Bey, R.M. Yantosca, A. Fiore, and Q. Li, Air mass factor formulation for spectroscopic measurements from satellites: Application to formaldehyde retrievals from the Global Ozone Monitoring Experiment *J. Geophys. Res., 104* 14,539-14,550, 2001.

Piccot, S.D., J.J. Watson, and J.W. Jones, A global inventory of volatile organic compound emissions from anthropogenic sources, *J. Geophys. Res., 97*, 9897-9912, 1992.

Pickering, K. E., et al., Convective transport of biomass burning emissions over Brazil during TRACE-A, *J. Geophys. Res., 101*, 23,993-24,012, 1996.

Prinn, R.G., R.F. Weiss, B.R. Miller, J. Huang, F.N. Alyea, D.M. Cunnold, P.J. Fraser, D.E. Hartley, and P.G. Simmonds, Atmospheric trends and lifetime of CH_3CCl_3 and global OH concentrations, *Science, 269*, 187-192, 1995.

Raper, J.L., M.M. Kleb, D.J. Jacob, D.D. Davis, R.E. Newell, H.E. Fuelberg, R.J. Bendura, J.M. Hoell, and R.J. McNeal, Pacific Exploratory Mission in the tropical Pacific: PEM-Tropics B, March-April 1999, *J. Geophys. Res.*, in press, 2001.

Rasch, P.J., et al., A comparison of scavenging and deposition processes in global models: Results from the WCRP Cambridge Workshop of 1995, *Tellus, 52*, 1025-1056, 2000.

Reissell, A., C. Harry, S.M. Aschmann, R. Atkinson, and J. Arey, Formation of acetone from the OH radical- and O_3-initiated reactions of a series of monoterpenes, *J. Geophys. Res., 104*, 13,869-13,879, 1999.

Rind, D., and J. Lerner, Use of on-line tracers as a diagnostic tool in general circulation model development, 1, Horizontal and vertical transport in the troposphere, *J. Geophys. Res., 101*, 12,667-12,683, 1996.

Roelofs, G.J., J. Lelieveld, and R. van Dorland, A three-dimensional chemistry/general circulation model simulation of anthropogenically derived ozone in the troposphere and its radiative forcing, *J. Geophys. Res., 102*, 23,389-23,401, 1997.

Rudolph, L., The tropospheric distribution and budget of ethane, *J. Geophys. Res., 100*, 11,369-11,381, 1995.

Schneider, H.R., D.B.A. Jones, G.-Y. Shi, and M.B. McElroy, Analysis of residual mean transport in the stratosphere, 1, Model description and comparison with satellite data, *J. Geophys. Res., 105*, 19,991-20,011, 2000.

Schubert, S.D., R.B. Rood, and J. Pfaendtner, An assimilated data set for earth science applications, *Bull. Amer. Meteorol. Soc., 74*, 2,331-2,342, 1993.

Schultz, M., D.J. Jacob, J.D. Bradshaw, S.T. Sandholm, J.E. Dibb, R.W. Talbot, and H.B. Singh, Chemical NO_x budget in the upper troposphere over the tropical South Pacific, *J. Geophys. Res., 105*, 6,669-6,679, 2000.

Singh, H.B., et al., Latitudinal distributions of reactive nitrogen in the free troposphere over the Pacific Ocean in late winter/early spring, *J. Geophys. Res., 103*, 28,237-28,246, 1998.

Singh, H.B., A.M. Thompson, and H. Schlager, SONEX airborne mission and coordinated POLINAT-2 activity: Overview and accomplishments, *Geophys. Res. Lett., 26*, 3053-3056, 1999.

Singh, H.B., et al., Distributed and fate of select oxygenated organic species in the troposphere and lower stratosphere over the Atlantic, *J. Geophys. Res., 105*, 3795-3805, 2000a.

Singh, H.B., Y. Chen, A.C. Staudt, D.J. Jacob, D.R. Blake, B.G. Heikes, and J. Snow, Dominant presence of oxygenated organic species in the remote southern Pacific troposphere, *Nature, 410*, 1078-1081, 2000b.

Spivakovsky, C.M., R. Yevich, J.A. Logan, S.C. Wofsy, and M.B. McElroy, Tropospheric OH in a three-dimensional chemical tracer model: An assessment based on observations of CH_3CCl_3, *J. Geophys. Res., 95*, 18441-18,471, 1990.

Spivakovsky, C.M., et al., Three-dimensional climatological distribution of tropospheric OH: Update and evaluation, *J. Geophys. Res., 105*, 8931-8980, 2000.

Toon, O.B., and R.C. Miakelye, Subsonic aircraft - contrail and cloud effects special study (SUCCESS), *Geophys. Res. Lett., 25*, 1109-1112, 1998.

United Nations, 1996 energy statistics yearbook, Stat. Div., U. N. Dep. for Econ. and Soc. Inf. and Pol. Anal., New York, 1998.

Wesely, M.L., Parameterization of surface resistance to gaseous dry deposition in regional-scale numerical models, *Atmos. Environ., 23*, 1293-1304, 1989.

Wild, O., Q. Zhu, and M.J. Prather, Fast-J: Accurate simulation of in- and below-cloud photolysis in global chemical models, *J. Atmos. Chem., 37*, 245-282, 2000.

World Meteorological Organization (WMO), Scientific assessment of ozone depletion: 1998, *Rep. 44*, Global Ozone Obs. Syst., Geneva, Switzerland, 1998.

I. Bey, Swiss Federal Institute of Technology (EPFL), DGR-LPAS, CH-1015 Lausanne, Switzerland. (e-mail: isabelle.bey@epfl.ch)

B. D. Field, A. M. Fiore, D. J. Jacob, Q. Li, H. Y. Liu, J. A. Logan, L. J. Mickley, R. M. Yantosca, Division of Engineering and Applied Sciences and Department of Earth and Planetary Sciences, Harvard University, 29 Oxford St., Cambridge, MA 02138. (e-mail: bdf; amf; djj; qli; hyl; jal; ljm; bmy@io.harvard.edu)

M. G. Schultz, Max-Planck-Institut für Meteorologie, Bundesstr. 55, D-20146 Hamburg, Germany. (e-mail: martin.schultz@dkrz.de)

(Received December 20, 2000; revised April 16, 2001; accepted April 27, 2001.)